SCIENTIFIC REPORTS

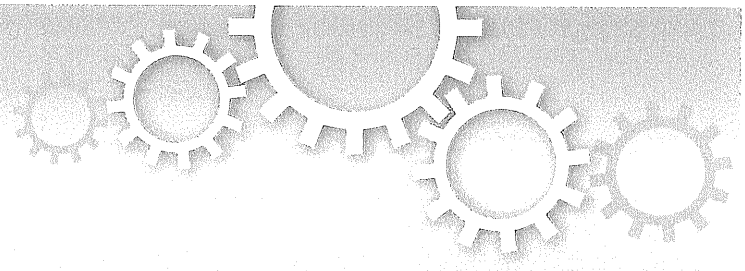

OPEN

SUBJECT AREAS:
PROTEIN DELIVERY
MESENCHYMAL STEM CELLS
MOLECULAR NEUROSCIENCE
PROTEASES

Received
17 October 2012

Accepted
15 January 2013

Published
1 February 2013

Correspondence and requests for materials should be addressed to T.O. (tochiya@ncc.go.jp)

Human adipose tissue-derived mesenchymal stem cells secrete functional neprilysin-bound exosomes

Takeshi Katsuda[1,2], Reiko Tsuchiya[3], Nobuyoshi Kosaka[1], Yusuke Yoshioka[1], Kentaro Takagaki[3], Katsuyuki Oki[3], Fumitaka Takeshita[1], Yasuyuki Sakai[2], Masahiko Kuroda[4] & Takahiro Ochiya[1]

[1]From the Division of Molecular and Cellular Medicine, National Cancer Center Research Institute, 5-1-1 Tsukiji, Chuo-ku, Tokyo 104-0045, Japan, [2]Institute of Industrial Science (IIS), The University of Tokyo, 4-6-1 Komaba, Meguro-ku, Tokyo 153-8505, Japan, [3]Research and Development Dept., SEEMS Inc., 2-4-32 Aomi, Koto-ku, Tokyo 135-0064, Japan, [4]Department of Pathology, Tokyo Medical University, 6-1-1, Shinjuku, Shinjuku-ku, Tokyo, 160-8402, Japan.

Alzheimer's disease (AD) is characterized by the accumulation of β-amyloid peptide (Aβ) in the brain because of an imbalance between Aβ production and clearance. Neprilysin (NEP) is the most important Aβ-degrading enzyme in the brain. Thus, researchers have explored virus-mediated NEP gene delivery. However, such strategies may entail unexpected risks, and thus exploration of a new possibility for NEP delivery is also required. Here, we show that human adipose tissue-derived mesenchymal stem cells (ADSCs) secrete exosomes carrying enzymatically active NEP. The NEP-specific activity level of 1 μg protein from ADSC-derived exosomes was equivalent to that of ~ 0.3 ng of recombinant human NEP. Of note, ADSC-derived exosomes were transferred into N2a cells, and were suggested to decrease both secreted and intracellular Aβ levels in the N2a cells. Importantly, these characteristics were more pronounced in ADSCs than bone marrow-derived mesenchymal stem cells, suggesting the therapeutic relevance of ADSC-derived exosomes for AD.

Alzheimer's disease (AD) is a progressive and fatal neurodegenerative disorder that is characterized by memory loss and cognitive ability deterioration. The accumulation of β-amyloid peptide (Aβ) in the brain plays a critical role in AD pathogenesis[1,2]. The steady-state level of Aβ is determined by a balance between its biosynthesis and clearance[3]. The physiological metabolite Aβ is constantly produced and removed in the brain, and it has been demonstrated that even small decreases in its removal lead to Aβ deposition[3]. Among several proteases involved in the proteolysis of Aβ, neprilysin (neutral endopeptidase: NEP), a type II membrane-associated metalloendopeptidase, appears to be the most important[4,5]. Indeed, AD patients show decreased expression and activity of NEP[6]. Thus, NEP has been intensively studied as a potential therapeutic target for AD[7]. One promising approach for lowering brain Aβ levels is the delivery of NEP. Recent reports have indicated that NEP gene delivery either peripherally or within the brain is effective in clearing brain Aβ[7]. However, safety issues related to the use of viral vectors limit the feasibility of this approach.

NEP, more often referred to as CD10, is expressed by mesenchymal stem cells (MSCs)[8,9]. However, to our knowledge, no study has explored the therapeutic potential of MSCs with regard to their Aβ degrading capacity. MSCs initially attracted interest for their ability to differentiate into cells of mesodermal lineage *in vitro* and *in vivo*[11]. Furthermore, in the last decade, it has been demonstrated that MSCs have many other functional properties. They can differentiate into cells from unrelated germline lineages, resist immunosurveillance, home to injured tissue, and secrete factors with immunosuppressive, anti-apoptotic, and trophic effects[10,11]. Accordingly, there is growing evidence that MSC-based therapies could benefit a wide range of neurodegenerative diseases[12], including AD[13–18]. The mechanisms by which transplanted MSCs influence AD have been roughly classified as cellular replacement[13,14] or paracrine secretion[15–18], but the precise mechanism remains unclear. Thus, any possible mechanism of AD pathophysiology should be investigated, and any possible strategy for AD treatment should be explored.

Another recently reported remarkable feature of MSCs is their ability to secrete exosomes with therapeutic potential[19]. Exosomes are small, intraluminal vesicles of multivesicular bodies released when they fuse with the plasma membrane[20]. It has been suggested that these vesicles are produced by a variety of cell types and can function as intercellular transmitters of mRNA, microRNA, and proteins[21–23]. The first evidence of the

therapeutic potential of MSC-derived exosomes was in a mouse model of acute kidney injury[24]. Bruno et al. found that bone marrow-derived (BM−) MSC exosomes activated a proliferative program in surviving tubular cells after injury via a horizontal transfer of mRNA. Lai et al. also reported that MSC-derived exosomes exerted therapeutic effects on myocardial ischemia/reperfusion injury[25].

Given that exosomes are membrane vesicles and that MSCs express membrane-bound enzyme NEP, it can be assumed that MSCs would secrete exosomes with NEP on their membrane. Here, we report for the first time that adipose tissue-derived MSCs (ADSCs) produce NEP-bound exosomes approximately 100–200 nm in diameter. Furthermore, co-culture of N2a cells overproducing human Aβ with ADSCs led to decreases in the secreted Aβ40 and 42 levels as well as a decrease in the intracellular Aβ42 level. Importantly, these characteristics were more pronounced in ADSCs than BM-MSCs, suggesting the therapeutic relevance of ADSC-derived exosomes for AD.

Results

ADSCs express NEP at a higher level than BM-MSCs. To select the optimal source of MSCs for the present study, we performed comparative analyses on NEP expression between ADSCs and BM-MSCs. A flow cytometry analysis indicated that NEP-positive populations in ADSCs were greater than those in BM-MSCs (Fig. 1A); regarding the other surface markers, they showed the similar profiles that are characteristic to MSCs (positive for CD105, CD73, CD90, and CD44; negative for CD45, CD31, and CD34) (Fig. S1). By qRT-PCR analysis, we confirmed that NEP gene expression levels were considerably higher in ADSCs from each donor than in BM-MSCs from all 4 donors (Fig. 1B). In addition, immunoblot analysis revealed that the NEP protein expression level in ADSCs was ~ 4-fold higher than that of BM-MSCs (Fig. 1C). This observation was further confirmed by immunocytochemistry, where ADSCs were stained for NEP more strongly than BM-MSCs (Fig. 1D). Collectively, these results demonstrate that ADSCs express more NEP than BM-MSCs. Thus, we mainly focused on ADSCs for the subsequent experiments.

ADSC-derived NEP exhibits specific enzyme activity. To investigate the feasibility of using ADSC-derived NEP as a therapeutic target, we examined whether ADSCs indeed exhibited NEP-specific enzyme activity. We measured NEP-specific enzyme activity using a fluorogenic peptide substrate, Mca-RPPGFSAFK(Dnp), and a selective NEP inhibitor, thiorphan. This substrate can be cleaved by several endopeptidases, including NEP, endothelin-converting enzyme (ECE)-1, ECE-2, angiotensin-converting enzyme (ACE)-1, ACE-2, and insulin-degrading enzyme (IDE)[26]. However, at pH 7.5, the use of thiorphan allows the discrimination of NEP enzyme activity from other closely related enzymes[26].

Cell lysates of ADSCs from each donor exhibited enzyme activity both in the presence and absence of thiorphan (Figs. S2 A-D). NEP-specific activity, calculated after the subtraction of fluorescence in the presence of thiorphan, demonstrated that all ADSCs exhibited NEP-specific enzyme activity (Fig. 2A). NEP-specific enzyme activity accounted for 38.3 ± 4.5% of total enzyme activity (Fig. 2B), and the activity level of 1 μg ADSC cell lysate was estimated to be equivalent to that of 0.35 ± 0.14 ng recombinant human NEP (rhNEP) (Fig. 2C, termed as NEP activity index). In contrast to the above observation, BM-MSCs showed weak or undetectable NEP enzyme activity (Fig. 2D). Intriguingly, the total enzyme activity of BM-MSCs measured in the absence of thiorphan was comparable to that of ADSCs (Figs. S3 A, B). That is, NEP-specific enzyme activity contributed relatively little to the total enzyme activity of BM-MSCs (Fig. 2D), suggesting that NEP activity is a unique characteristic of ADSCs. These results support the idea that NEP expressed by ADSCs, but not BM-MSCs, may be therapeutically useful for AD.

ADSCs secrete exosomes to their culture supernatant. Recently, it has been shown that exosomes secreted by MSCs contribute to their paracrine effects[19,25,26]. Considering the reports that transplanted MSCs influenced AD via their paracrine effects[15–18], we hypothesized that ADSC-derived exosomes would have therapeutic potential for AD, especially by focusing on their NEP producing ability.

To test whether ADSCs could secrete NEP via exosome release, we isolated putative exosome fractions from conditioned media of ADSCs from 4 donors (#1–4) with a standard ultracentrifugation method[27,28]. The phase-contrast electron micrographs of the exosomes revealed rounded and double-membraned structures with a size of approximately 60–200 nm (Fig. 3A). Immunoblot analyses revealed that tetraspanin CD81, a reliable exosomal marker[29], was present in the exosome fraction but absent in the donor cell lysates (Fig. 3B). We also confirmed the presence of CD63, another well-established exosome marker[29] (Fig. 3B). CD63 was also detected in the cell lysate, but this is in accordance with the fact that CD63 is expressed by MSCs[30]. In contrast, cellular proteins cytochrome c and actin were detected exclusively in the cell lysates (Fig. 3B). Then, we analyzed the size distribution of the isolated exosomes by two distinct methods: NTA and scanning ion occlusion sensing (SIOS). The size distribution was physically homogeneous with a peak at 150–200 nm, as determined by nanoparticle tracking analysis (NTA) (Fig. 3C, E), or at 110–160 nm, as determined by SIOS (Fig. 3D, E). The size of ADSC-derived exosomes was relatively larger than that of previously reported exosomes, which were 50–100 nm in diameter. The exosome yield per 10^6 ADSCs per day was 1–4 × 10^8 particles, as determined by NTA, or 1–4 μg protein, as determined by the Bradford method (Fig. 3E). Collectively, these results reveal that ADSCs secrete exosomes to the culture supernatant.

ADSC-derived exosomes contain enzymatically active NEP. It is thought that the molecular composition of exosomes reflects the specialized functions of their original cells[19,31]. Thus, we next asked whether ADSC-derived exosomes contained enzymatically active NEP. Immunoblot analyses revealed that exosomes secreted by each line of donor-derived ADSCs contained NEP (Fig. 4A). Of note, the enzyme activity assay using a fluorogenic substrate revealed that these exosomes exhibited NEP-specific activity (Fig. 4B). Interestingly, comparison of exosomal enzyme activity in the presence and absence of thiorphan demonstrated that NEP-specific activity accounted for a large proportion of the total activity (Fig. 4C, D): the enzyme activity was almost completely lost in the presence of thiorphan (Fig. 4D). The NEP-specific activity / total activity ratios of ADSC-derived exosomes reached 89.5 ± 4.4% (Fig. 4E). NEP-specific activity level of 1 μg protein from ADSC-derived exosomes was estimated to be equivalent to 0.26 ± 0.07 ng rhNEP (Fig. 4F, Fig. 4S). In addition, we confirmed that ADSC-derived exosomes exhibited a higher NEP-specific activity than BM-MSC-derived esosomes (Fig. 4G). These results demonstrate that ADSC-derived exosomes possess enzymatically active NEP, implying that they can serve as a novel NEP protein delivery system.

ADSCs decrease both the extracellular and intracellular Aβ levels of N2a cells. To test whether ADSCs could contribute to decrease of both synthesized and secreted Aβ, we co-cultured ADSCs or BM-MSCs with a neuroblastoma cell line N2a cells genetically modified to overproduce human Aβ (Fig. 5A)[32]. Both Aβ40 and 42 levels in the N2a cell culture media were significantly decreased after co-culture with ADSCs or BM-MSCs (Fig. 5B, C). The decreasing degrees of both secreted Aβ40 and 42 levels were greater in co-culture with ADSCs than BM-MSCs (Fig. 5B, C). Of note, we also found that

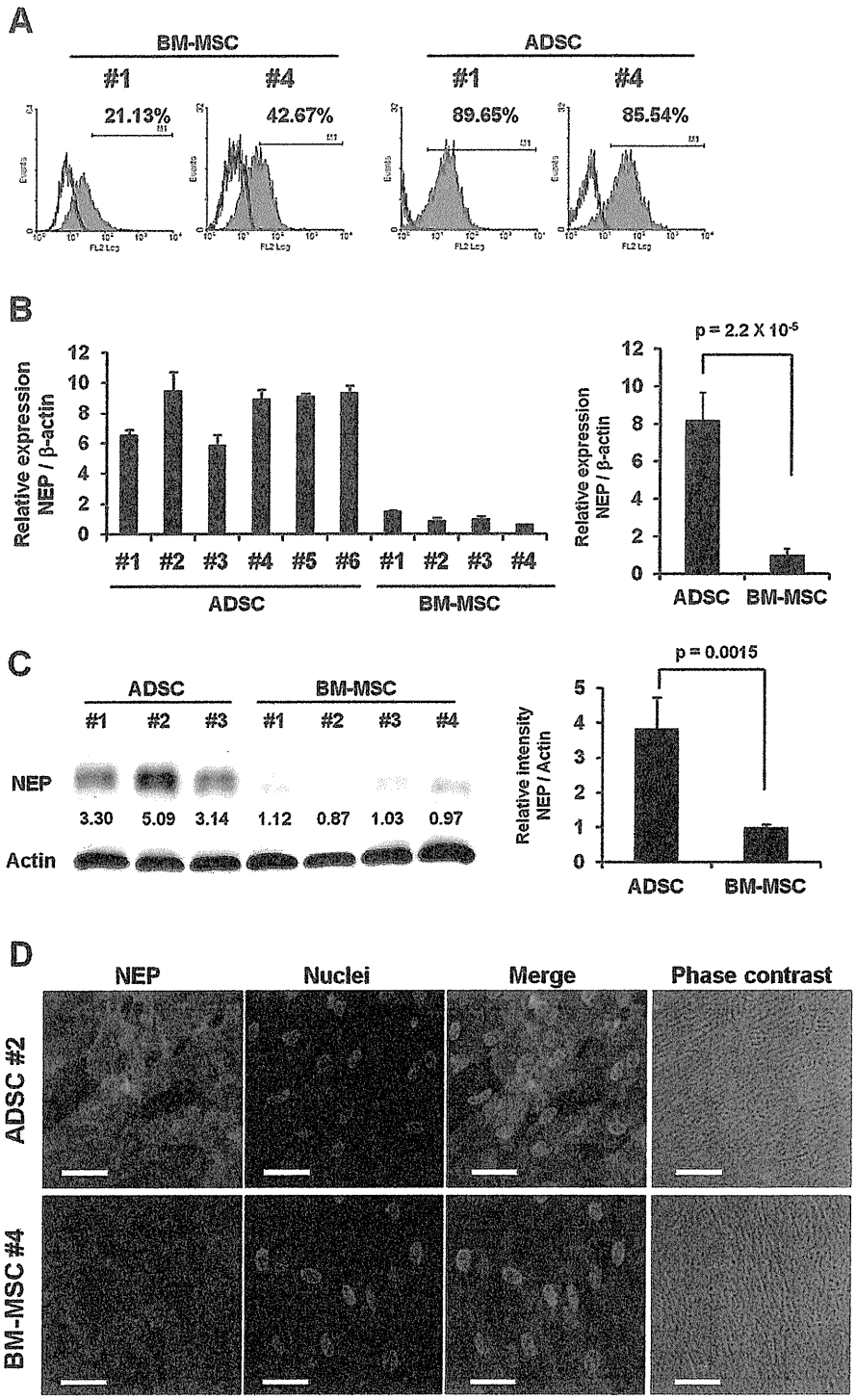

Figure 1 | ADSCs express NEP at a higher level than BM-MSCs. (A) Flow cytometry results of ADSCs #1 and #4 and BM-MSCs #1 and #4 for NEP. (B) qRT-PCR analysis of NEP in ADSCs and BM-MSCs. Transcript levels were normalized to β-actin levels. Data are the mean ± S.D. (n = 3). (C) Cell lysates of ADSCs or BM-MSCs were analyzed by immunoblotting with an anti-NEP or an anti-actin antibody (left). Either 3 μg or 1 μg of cell lysate protein per lane was loaded for NEP and actin, respectively. The relative signal intensity (NEP/Actin) for each sample was measured, and normalized values are shown in the graph. The average values of ADSCs and BM-MSCs are compared on the right. Data are the mean ± S.D. (D) Immuno cytochemistry of ADSCs for NEP. ADSCs were stained with a mouse-anti NEP monoclonal antibody (green), and nuclei were counterstained with Hoechst 33342 (blue). Scale bar: 50 μm.

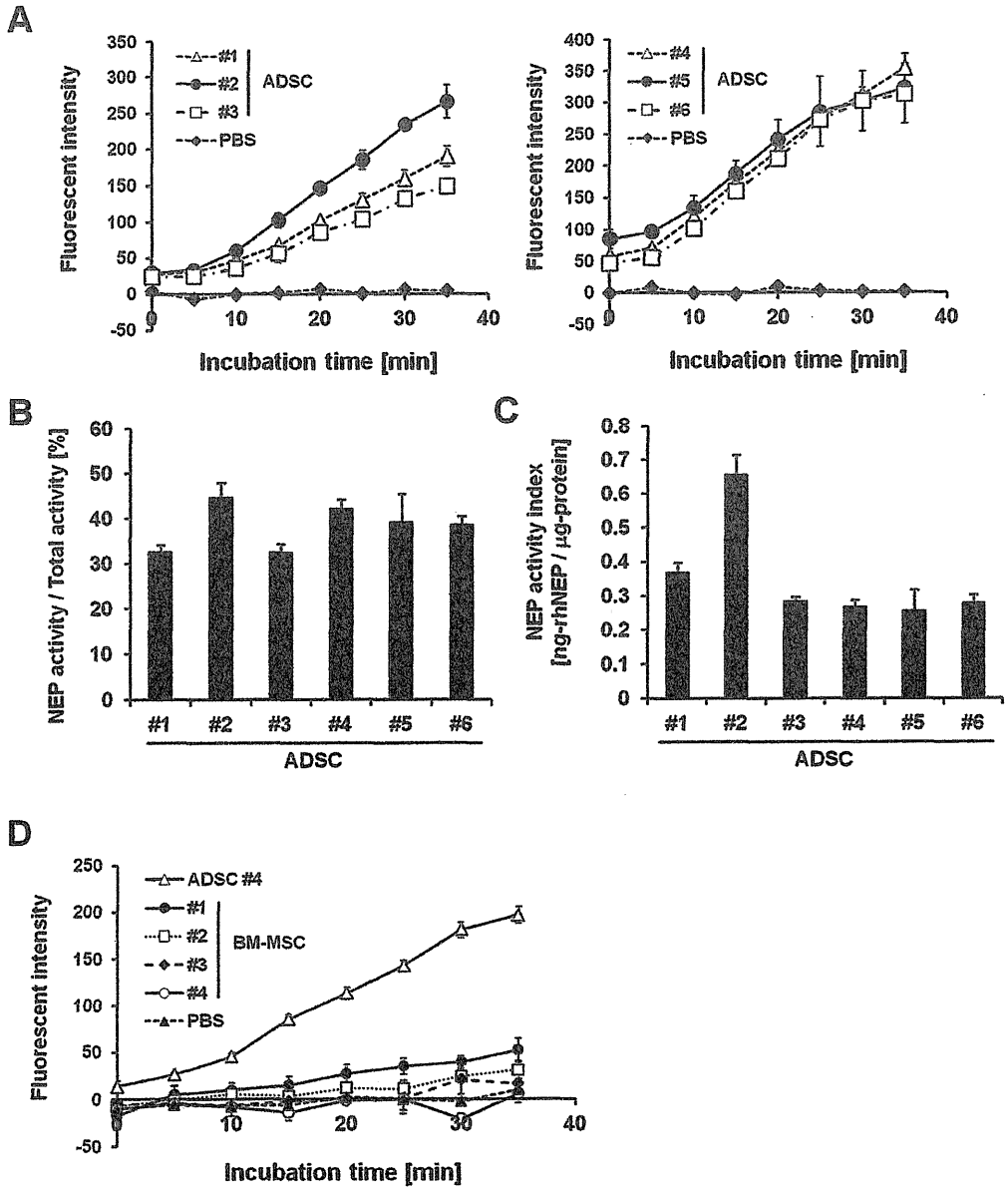

Figure 2 | ADSCs, but not BM-MSCs, exhibit NEP-specific enzyme activity. (A) NEP-specific enzyme activity was measured in ADSC cell lysates (left: #1–3 and right: #4–6) using a fluorogenic peptide substrate, Mca-RPPGFSAFK(Dnp). The average NEP activity represented by fluorescence intensity was measured with a reading interval of 5 min. The specific NEP activity was calculated by subtracting residual fluorescent intensity after incubation with the NEP inhibitor thiorphan (Fig. S2 A–D). Data are the mean ± S.D. (n = 3). (B) NEP contribution ratio calculated as the percentage ratio of NEP-specific activity rate to total activity rate. NEP-specific or total enzyme activity rate was determined as the gradient of the corresponding time course of fluorescent intensity. Data are the mean ± S.D. (n = 3). (C) NEP-specific enzyme activity levels of ADSCs were estimated from rhNEP standard curves (Fig. S2 E–H) and represented as the value ng-rhNEP/μg-protein (termed as NEP activity index in the diagram). Data are the mean ± S.D. (n = 3). (D) Comparison of NEP-specific enzyme activity levels between ADSC #4 and BM-MSCs #1–4. Data are the mean ± S.D. (n = 3).

the intracellular Aβ42 level in N2a cells was significantly decreased by co-culture with ADSCs or BM-MSCs (Fig. 5D). This suggests that NEP-loaded exosomes secreted by ADSCs or BM-MSCs entered the cytoplasm of N2a cells, and degraded the intracellular Aβ of N2a cells. Indeed, addition of thiorphan raised the intracellular Aβ42 level from 77% to 92% of that of the control (Fig. 5E). We also confirmed that ADSC-derived exosomes, at least in part, contributed to decreasing the intracellular Aβ42 level in N2a cells (Fig. S5).

ADSC-derived exosomes are incorporated into neuroblastoma cells. To verify that ADSC transferred their exosomes to N2a cells, we co-cultured PKH26 labeled ADSCs with PKH67 labled N2a cells (Fig. 6A). One day after co-culture, some, but not all, N2a cells were co-stained with PKH26 and PKH67, suggesting that exosomes secreted by ADSCs were transferred to N2a cells (Fig. 6A). Interestingly, however, we did not observe co-stained ADSCs, suggesting a certain mechanism underlying the unidirectional transport of exosomes from ADSCs to N2a cells, but not from N2a cells to ADSCs. Exosomal membrane is rich in ceramide, which may lead to inefficient incorporation of the cell membrane-linked PKH into the secreted exosomes[33]. Thus, we next directly labeled ADSC-derived exosomes with PKH67, and examined whether these

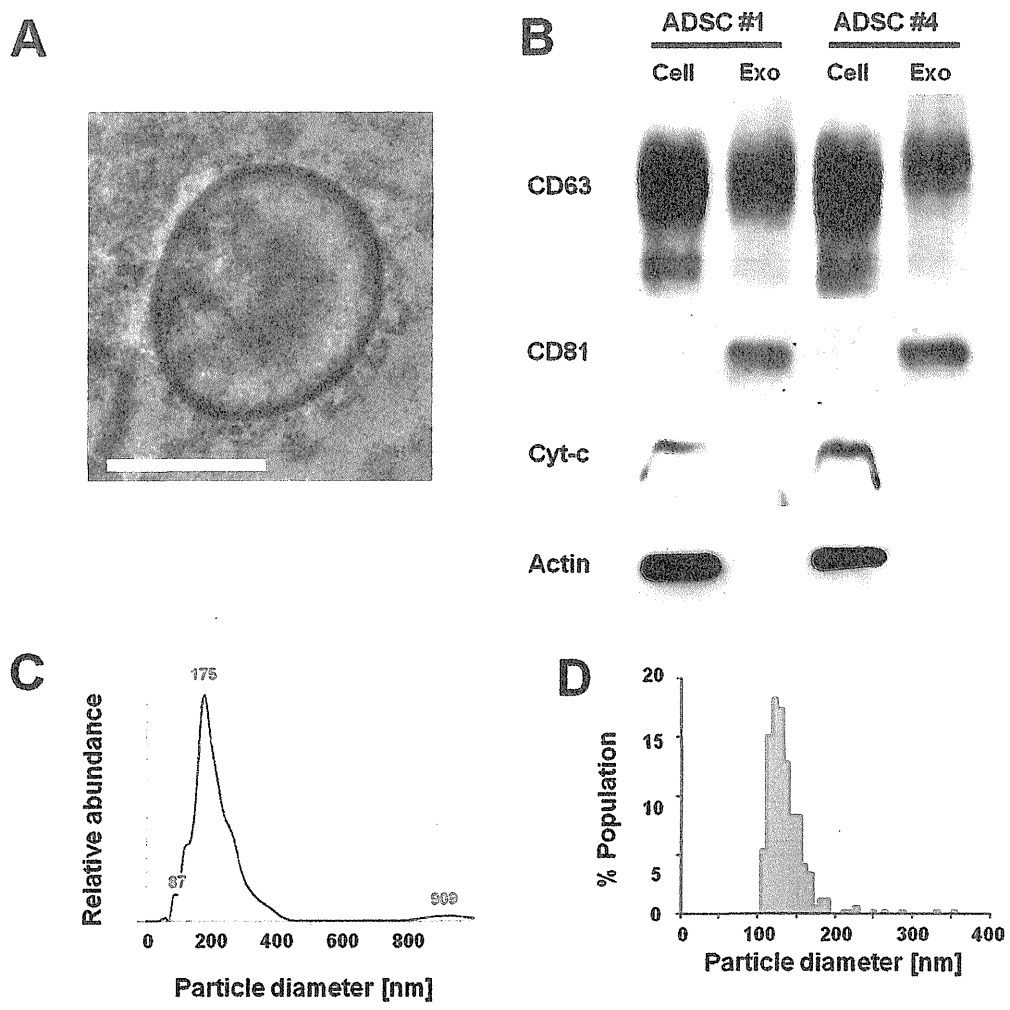

E

		Yield [/ 10^6 cells / d]		Peak diameter [nm]	
		Protein [μg]	X 10^8 Particles	By NTA	By SIOS
ADSC	#1	3.5 ± 1.6	3.2 ± 1.6	175	118.9
	#2	2.8 ± 1.5	1.4 ± 0.26	169	127.8
	#3	1.7 ± 0.55	1.6 ± 0.56	136	—
	#4	3.8 ± 1.1	—	160	117.3

Figure 3 | ADSCs secrete 100–200 nm exosomes. (A) A phase-contrast transmission electron micrograph of purified ADSC #4-derived exosomes. Scale bar: 100 nm. (B) The exosome fractions and cell lysates of ADSCs #1 and #4 were analyzed by immunoblotting with antibodies against exosomal proteins CD63 and CD81 and cellular proteins cytochrome-c (Cyt-c) and actin (CD63 under nonreducing conditions). Equal amounts of protein from cell lysates or exosomes were used for each assay: 0.5 μg for CD63, 5 μg for CD81 and Cyt-c, and 1 μg for actin. (C, D) Size distribution of ADSC#1-derived exosomes as measured by nanoparticle tracking analysis (NTA) showed a peak at 175 nm (C), and scanning ion occlusion sensing (SIOS) showed a peak at 118.9 nm (D). (E) Yields and peak diameters of exosomes produced by ADSCs #1–4 are summarized. Protein amounts and particle numbers of harvested exosomes were determined by the Bradford method and NTA, respectively. Peak diameters were determined by NTA and SIOS. Data are the mean ± S.D. (n = 3–4).

exosomes were incorporated into N2a cells (Fig. 6B). Seven hr after exosome addition to N2a culture medium, some of the cells were already stained green. Furthermore, after 24 hr, most N2a cells were stained green, indicating that ADSC-derived exosomes were efficiently transferred into recipient N2a cells. Collectively, it was demonstrated that ADSCs transferred their exosomes to N2a cells, which may lead to the decrease in the intracellular Aβ42 level of N2a cells.

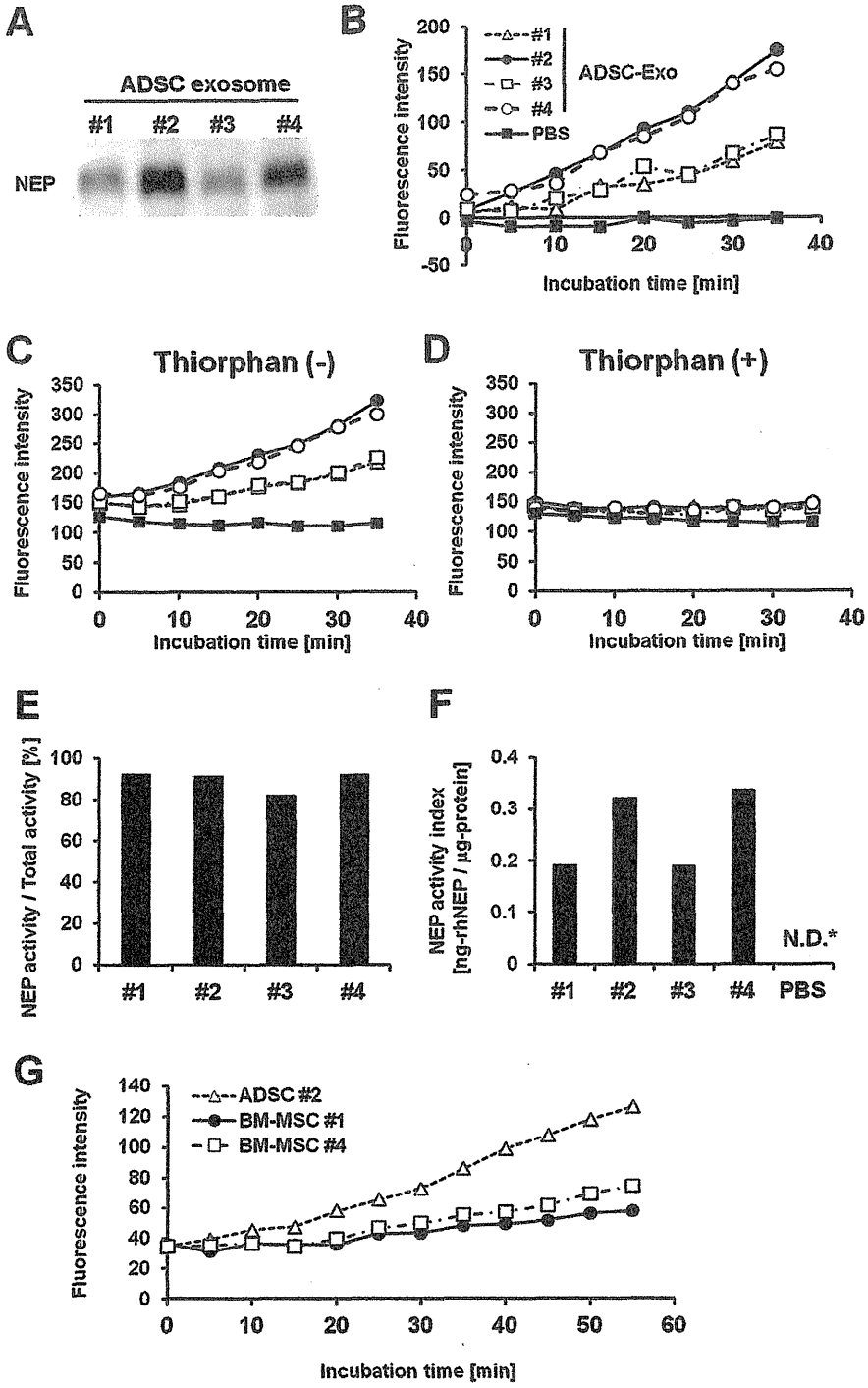

Figure 4 | ADSC-derived exosomes possess enzymatically active NEP. (A) Immunoblotting for NEP of exosomes isolated from ADSCs #1–4. (B–D) NEP enzyme activity assay for ADSC-derived exosomes (#1–4). NEP enzyme activity was measured using a fluorogenic peptide substrate, Mca-RPPGFSAFK(Dnp) and NEP inhibitor thiorphan. NEP specific activity (B) was calculated by subtracting the residual fluorescence intensity measured in the presence of thiorphan (D) from the total enzyme activity measured in the absence of thiorphan (C). Addition of thiorphan sharply reduced the enzyme activity of ADSC-derived exosomes (D). (E) NEP contribution ratio for ADSC-derived exosomes calculated as the percentage ratio of NEP-specific activity rate to total activity rate. (F) NEP-specific enzyme activity levels of exosome fractions of ADSCs #1–4 were estimated from a rhNEP standard curve (Fig. 4S) and are represented as the value ng-rhNEP/μg protein (termed as NEP activity index in the diagram). N.D. indicates "not determined".

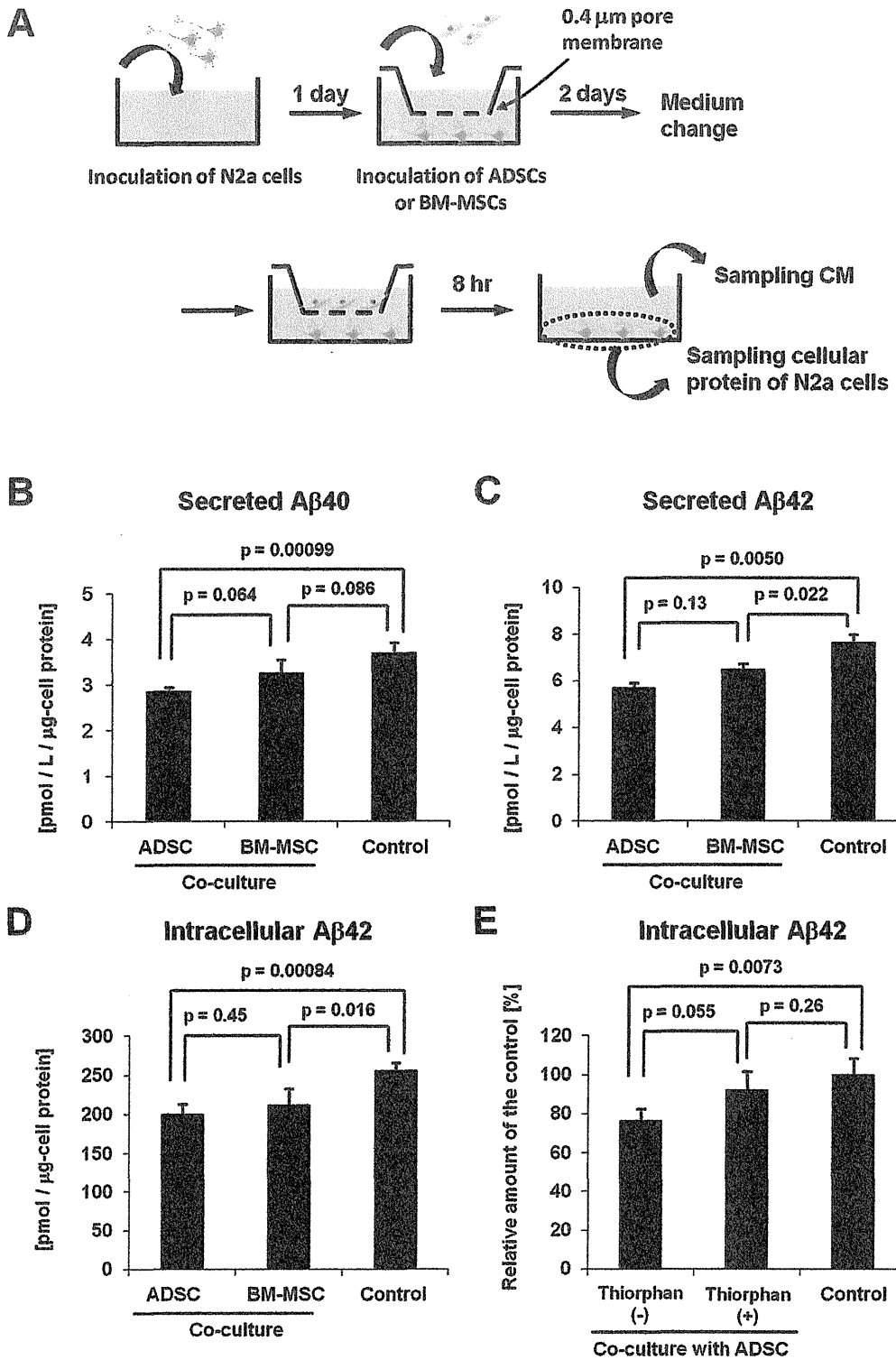

Figure 5 | ADSCs decrease both the extracellular and intracellular Aβ levels of N2a cells. (A) Schematic representation of the co-culture experiments of N2a cells with ADSCs or BM-MSCs using cell culture inserts. Secreted Aβ40 (B) and Aβ42 (C) levels were measured using the collected CM in the bottom chambers by ELISA. Each value was normalized to the protein content of N2a cell lysates. Data are the mean ± S.D. (n = 4). (D) Intracellular Aβ42 levels were measured using the N2a cell lysates by ELISA. Each value was normalized to the protein content of N2a cell lysates. (E) Intracellular Aβ42 levels were compared in co-cultures of ADSCs and N2a cells in the presence and absence of thiorphan. Each value is shown as the relative level to the control. Data are the mean ± S.D. (n = 4).

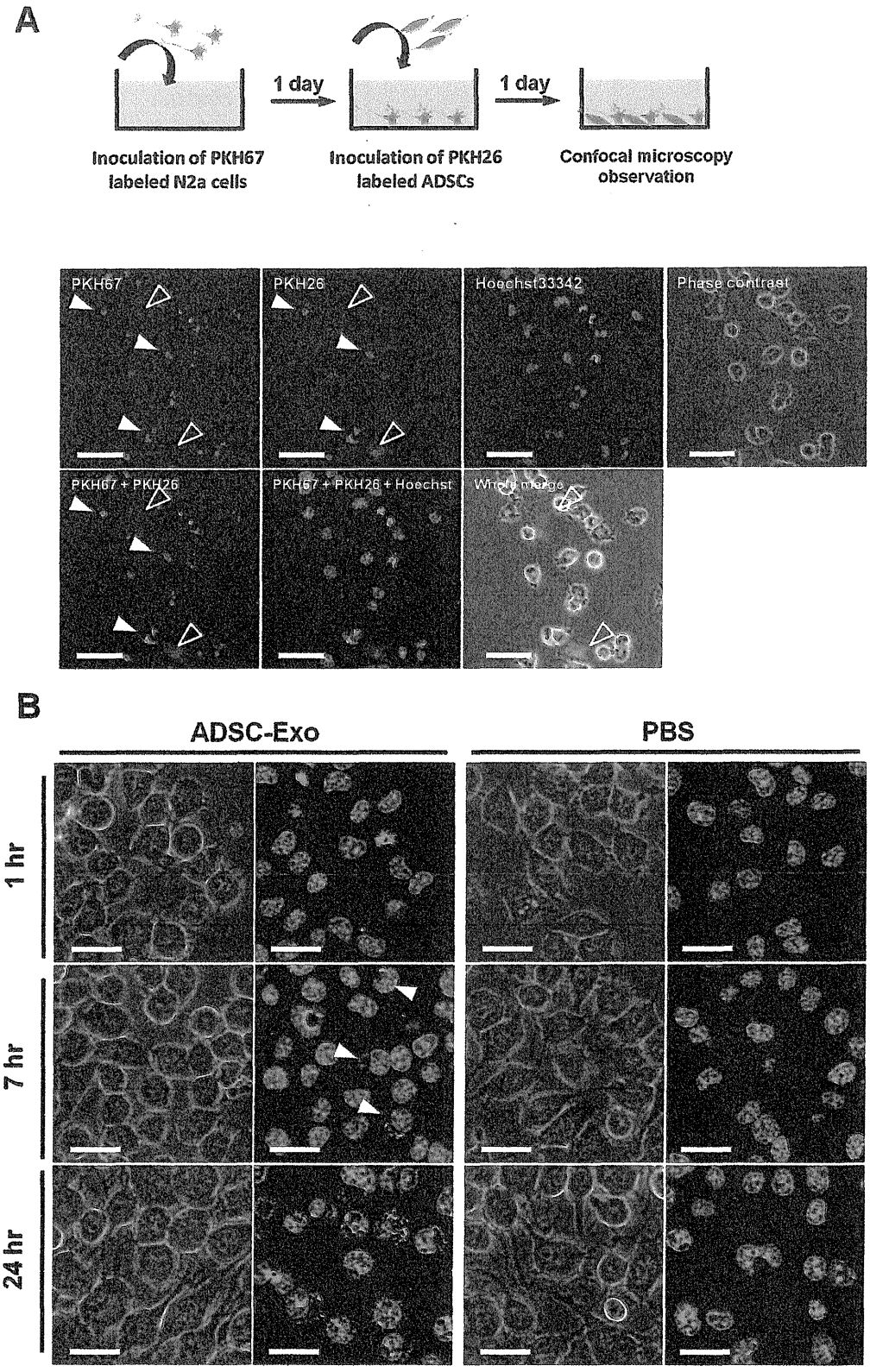

Figure 6 | ADSC-derived exosomes are incorporated into N2a cells. (A) Top diagram shows the schematic representation of the co-culture experiements of N2a cells and ADSCs labeled with PKH67 and PKH26, respectively. Bottom diagram shows the representative image taken 24 hr after co-culture of N2a cells with ADSCs. Filled arrowheads indicate N2a cells co-stained with PKH26 and PKH67. Open arrowheads indicate PKH26 labeled ADSCs. Scale bar: 50 μm. (B) Purified ADSC exosomes or vehicle PBS(-) as a control were labeled with PKH67, and incubated with cultured N2a cells. 7 hr after incubation, some of the cells were stained green (arrowheads). After 24 hr, most N2a cells were stained green. Scale bar: 25 μm.

Discussion

In this study, we demonstrated the unique potential of ADSCs for AD treatment. The main finding was that ADSCs secreted functional NEP in association with exosomes. Most importantly, these ADSC-derived exosomes exhibited NEP-specific enzyme activity. Furthermore, it was indicated that exosomes secreted by ADSCs were transferred to N2a cells, and contributed, at least in part, to decrease of both extracellular and intracellular Aβ levels. Another important observation was that ADSCs expressed NEP at a higher level than BM-MSCs. These results suggest that ADSCs may serve as a promising cell source for exosome-based AD treatments.

To our knowledge, this is the first report of the isolation of exosomes containing functional NEP from cultured cells, suggesting a promising new approach for AD treatment. Earlier studies have shown that NEP is present in microvesicles derived from certain body fluids, including prostatic fluid[34], epididymal fluid[35], and urine[36]. However, no study has focused on the therapeutic potential of microvesicle-bound NEP for AD. Indeed, it seems impractical to obtain a sufficient amount of microvesicles from the limited amount of available body fluid. In this context, MSCs have a great advantage because they can be isolated in large amounts from patients and they have the ability to expand many-fold in culture. Importantly, the co-culture experiments suggested that ADSC-derived exosomes contributed to decrease of the secreted Aβ level in N2a cells. Furthermore, it is intriguing that the intracellular Aβ42 level was also decreased by co-culture with ADSCs as well as by addition of ADSC-derived exosomes. Although we do not exclude other possible effects of ADSCs on the co-cultured N2a cells, the results indicate a novel possibility: that is, incorporated ADSC-derived exosomes contributed to the degradation of the intracellular Aβ42 in the recipient N2a cells. Many reports have suggested that accumulation of intraneuronal Aβ42 is an early event in the progression of AD, preceding the formation of extracellular Aβ deposits[37]. Thus, our results suggest the possibility that ADSC-derived exosomes contribute to prevention of extracellular plaque formation and subsequent AD pathogenesis.

Our results also demonstrated that ADSCs, but not BM-MSCs, expressed enzymatically active NEP. Since the discovery of MSCs in bone marrow, MSCs have been identified in many adult tissues[8–10]. Although ADSCs and BM-MSCs are considered to be similar, an increasing number of reports have indicated that these cells have phenotypic differences regarding differentiation capacity[8], immunosuppressive potential[38,39], homing and migratory behavior[40], and trophic effects[39,41]. These observations highlight the importance of selecting the optimal mesenchymal tissue as a source of MSCs for specific purposes. In this context, our comparative analyses between ADSCs and BM-MSCs provide strong evidence that ADSCs are the more suitable source of NEP-bound exosomes.

Another interesting finding was that ADSC-derived exosomes were rich in NEP. The fluorogenic substrate used in the present study can be cleaved by NEP and closely related enzymes, including IDE, ECEs, and ACEs. All of these enzymes can degrade Aβ, although their contribution in Aβ clearance in the brain is small[4,5]. ECEs and ACEs are membrane-bound enzymes, suggesting their potential presence on secreted exosomes. However, the experiments with the NEP-specific inhibitor thiorphan revealed that ~ 90% of the enzyme activity of ADSC-derived exosomes was accounted for by NEP; the counterpart of the donor ADSC lysates was ~ 40%. Furthermore, we also found that BM-MSC-derived exosomes also exhibited NEP-specific activity. Intriguingly, whereas NEP-specific activity of parental BM-MSCs slightly contributed to the total enzyme activity, that of their exosomes accounted for more than 70% of the total enzyme activity (Fig. S6). We do not have an explanation for these observations, but it is likely that NEP was enriched in exosomes during their biogenesis. Collectively, these results suggest that ADSC-derived exosomes offer a new therapeutic approach to AD.

Recent reports support a scenario in which NEP-loaded exosomes contribute to Aβ clearance in the brain. A major obstacle for systemically administered drugs is the blood-brain barrier (BBB). Membrane vesicles have been proposed to be transported across the interior of a cell via transcytosis[42], which may enable these vesicles to cross the BBB. Indeed, recent reports have suggested that exosomes administered intravenously[43] or intranasally[44] crossed the BBB and resulted in successful delivery of the cargo directly into the brain. These studies strongly support the hypothesis that ADSC-derived exosomes can directly enter the brain and help clear extracellular Aβ. Another possibility is that ADSC-derived exosomes may help lower peripheral Aβ levels, which possibly promotes brain Aβ clearance. Peripheral degradation of Aβ through virus-mediated NEP gene delivery has been demonstrated to decrease brain soluble Aβ peptide levels[45,46]. In this context, NEP delivery using ADSC-derived exosomes has an advantage in patient safety because it does not require the use of viral vectors. Taken together, ADSC-derived exosomes may offer a promising approach to NEP delivery peripherally and/or directly into the brain.

In conclusion, this study proposes a new therapeutic approach to AD using ADSC-derived exosomes. Further work will be required to assess the utility of NEP-loaded exosomes for AD therapy.

Methods

Cell culture. ADSCs #1–3 were purchased from Invitrogen. ADSCs #4–6 were isolated in our laboratory by processing adipose tissue as previously described[11]. BM-MSCs #1–3 and #4 were purchased from the RIKEN cell bank and Cambrex, respectively. The donor information for ADSCs and BM-MSCs is listed in Supplementary Tables 1 and 2, respectively. BM-MSCs and ADSCs were routinely cultured in reduced serum (2%) medium (MesenPRO RS, Invitrogen) containing 1 × Glutamax (Invitrogen) and 1 × antibiotic antimycotic (Invitrogen). All ADSCs and BM-MSCs were used within the eighth passage. Stable mouse neuroblastoma N2a cells expressing both human APP695 with the Swedish mutation and presenilin 2 with the N141I mutation were kindly provided by Dr. Saido Takaomi (RIKEN Brain Institute, Japan). N2a cells were cultured in Dulbecco's modified Eagle's medium (Invitrogen) supplemented with 10% FBS (Invitrogen) and 1 × antibiotic antimycotic.

Flow cytometry. Aliquots of detached cells were washed in PBS containing 2% BSA and stained with anti-CD10 PE-conjugated (Biolegend). Samples were acquired using Cytomics FC500 flow cytometer (Beckman Coulter) and analyzed by CXP and WinMDI software.

Quantitative reverse transcription PCR (qRT-PCR). Total RNA was isolated from ADSCs and BM-MSCs with the RNeasy Mini Kit (QIAGEN). Reverse-transcription was performed using SuperScript III Reverse Transcriptase (Invitrogen, Tokyo, Japan) and random primers (Invitrogen) according to the manufacturer's guidelines. cDNAs were used for PCR utilizing Platinum SYBR Green qPCR SuperMix UDG (Invitrogen). NEP expression levels were normalized to an endogenous control, β-actin. The sequences of the NEP and β-actin primers (Invitrogen) were as follows: for NEP, 5′-CCTTCTTTAGTGCCCAGCAG-3′ (forward) and 5′- TGAGTCC ACCAGTCAACGAG-3′ (reverse); for β-actin, 5′- ACTCTTCCAGCCTTCC TTCC-3′ (forward) and 5′- AGCACTGTGTTGGCGTACAG-3′ (reverse).

Protein extraction. ADSCs and BM-MSCs were dissolved in Mammalian Protein Extraction Reagent (M-PER) (Pierce, Rockford, IL). Prepared cell lysates were used for immunoblotting and NEP enzyme activity assays. The protein concentrations were measured by the Bradford method using a protein assay kit (Bio-Rad).

Immunoblot analysis. Cell lysates and exosomes were separated on SDS-polyacrylamide gels and transferred to polyvinylidine difluoride membranes (BIORAD, Tokyo, Japan). Blots were blocked in blocking solution (Nacalai Tesque) at 4°C overnight and incubated at room temperature for 1 hour with mouse monoclonal anti-NEP (Abcam) (1 : 1000), mouse anti-actin (1 : 2000), mouse-anti CD63 (BD) (1 : 200), mouse-anti CD81 (Santa Cruz Biotechnology) (1 : 200), or mouse-anti cytochrome-c (BD) (1 : 200) antibody (CD63 was assessed under nonreducing conditions). Following washing in TBS-T, the membranes were incubated for 1 hour with sheep anti-mouse IgG-HRP-linked whole antibodies. Bound antibodies were visualized by chemiluminescence using an ECL Plus Western blotting detection system (RPN2132) (GE HealthCare) or an ImmunoStar kit (Wako), and images were analyzed by a LuminoImager (LAS-3000; Fuji Film, Inc.).

Immunocytochemistry. The cells were cultured in glass base dishes (IWAKI), and subsequently fixed in 4% paraformaldehyde (Sigma-Aldrich) in PBS. Heat-induced antigen retrieval was performed using ImmunoSavor (Nisshin EM Co. Ltd.). After incubation in blocking solution (Nacalai Tesque), the cells were incubated with

mouse monoclonal anti-NEP (Abcam) at 1 : 100 overnight at 4°C. Then, the cells were incubated with Alexa Fluor 488-conjugated goat anti-mouse IgG antibody (Invitrogen) at 1 : 500 for 60 min. Nuclei were counterstained with Hoechst 33342 (Dojindo).

Preparation of conditioned medium (CM) and exosomes. Prior to culture medium collection, ADSCs were washed twice with PBS, and the medium was switched to fresh serum-free medium (StemPRO SFM, Invitrogen). After incubation for 2–3 days, the medium was collected and centrifuged at 2,000 × g for 15 min at room temperature. The cells were supplemented with fresh SFM, cultured for 2–3 more days, and the medium was collected and centrifuged as described above. The harvested media were combined into 1 batch. To thoroughly remove cellular debris, the supernatant was filtered with a 0.22-μm filter unit (Millipore). Then, the CM was ultracentrifuged at 110,000 × g for 70 min at 4°C. The pellets were washed with 11 ml PBS, and after ultracentrifugation, they were resuspended in PBS. The exosome fraction protein content was assessed by the Bradford method.

NEP enzyme activity assay. Neprilysin activity was determined by fluorescence resonance energy transfer. The fluorogenic peptide substrate Mca-RPPGFSAFK(Dnp)-OH (R&D Systems, Inc.) was added at a final concentration of 20 μM to 5 μg cell lysates, and 5 or 10 μg ADSC-derived exosomes, respectively. The enzymatic reaction was carried out at 37°C in the presence or absence of the NEP inhibitor thiorphan (2.5 μg/mL) (Enzo Life Science). Fluorescent intensity was read at excitation and emission wavelengths of 320 nm and 405 nm, respectively, in kinetic mode for 5 minutes using a Safire Multi-Detection Monochrometer Microplate Reader (Tecan). The NEP-specific activity was determined as the fluorescence difference occurring in the presence or absence of thiorphan. NEP-specific or total enzyme activity rate was determined as the gradient of the corresponding time course of the fluorescent intensity. Then, the NEP contribution ratio was calculated as the percentage ratio of the NEP-specific activity rate and the total activity rate. We also quantified absolute NEP-specific activity using serial dilutions of recombinant human NEP (rhNEP) (R&D Systems, Inc.) as a standard. The gradient of the time course of the fluorescent intensity in its linear region was determined at each concentration of the rhNEP dilution series to produce a standard curve. NEP activity per sample protein amount was determined as the rhNEP-equivalent amount, which we termed as the "NEP activity index" with the unit ng-rhNEP/μg-sample protein.

Phase-contrast transmission electron microscopy. ADSC-derived exosomes were visualized by Terabase Inc. using the phase-contrast transmission electron microscopy, which can envision the high-contrast images of nano structures of soft-materials including biological samples such as liposomes, viruses, bacteria, and cells, without staining process which may cause damages on the subjects. The natural structure of the sample distributed in the solution can be observed by preparing the sample with rapid vitreous ice embedding method and using cryo phase-contrast transmission electron microscopy.

Measurement of size distribution and particle number by nanoparticle tracking analysis (NTA). NTA was carried out using the Nanosight system (NanoSight) on exosomes resuspended in PBS at a concentration of approximately 500 μg protein/mL and were further diluted 100-fold for analysis. The system focuses a laser beam through a suspension of the particles of interest. These are visualized by light scattering using a conventional optical microscope aligned perpendicularly to the beam axis, which collects light scattered from every particle in the field of view. A 60 s video records all events for further analysis by NTA software. The Brownian motion of each particle is tracked between frames, ultimately allowing calculation of the size through application of the Stokes-Einstein equation.

Size distribution analysis by scanning ion occlusion sensing (SIOS). SIOS analysis was carried out using the qNano system (Izon Science, Ltd.) on exosomes resuspended in PBS. SIOS allows single particle measurements as colloids and/or biomolecular analytes are driven through pores one at a time. Particles crossing the nanopore are detected as a transient change in the ionic current flow, which is denoted as a blockade event with its amplitude as the blockade magnitude. As blockade magnitude is proportional to particle size, accurate particle sizing can be achieved after calibration with a known standard.

Co-culture of N2a cells with ADSCs. For assessing whether MSCs can affect production and secretion of Aβ by N2a cells, we performed co-culture experiment using cell culture inserts possessing 0.4 μm pores (BD Falcon). N2a cells were seeded to the bottom chambers of 24 well-plates (BD Falcon) at 2 × 10^4 cells/well. On the next day, ADSCs #2 were seeded to the top chambers at 6 × 10^3 cells/insert which gave an almost confluent monolayer. After 2 days, culture media in the both top and bottom chambers were changed with fresh media, and the cells were cultured for further 8 hr. Then, the media in the bottom chambers were collected, centrifuged at 2,000 × g for 10 min, and the supernatants were used for the subsequent analysis. N2a cell lysates were also collected using M-PER, and cellular protein amounts were determined by Bradford method. Secreted and intracellular Aβ40 and 42 levels were measured using the CM and the N2a cell lysates, respectively, with ELISA kits (Wako). Both secreted and intracellular Aβ levels were normalized by the protein content of N2a cells. To investigate whether the decrease of Aβ levels was ascribed to NEP activity, thiorphan was added to the culture inserts at the concentration of 20 μM.

Exosome transfer analysis by co-culture experiments. N2a cells were labeled with a PKH67 green fluorescent labeling kit (Sigma-Aldrich) following the manufacture's instruction, and seeded to 35 mm glass base dishes (IWAKI) at 5 × 10^4 cells/dish. On the next day, ADSCs #2 were labeled with a PKH26 red fluorescent labeling kit (Sigma-Aldrich) and added to the dishes at 5 × 10^4 cells/dish (Fig. 5A). After 24 hr, cells were observed under confocal microscopy.

PKH67-labeled exosome transfer. Purified exosomes derived from ADSCs #2 CM were labeled with PKH67. Exosomes were incubated with 2 M PKH67 for 5 min, washed 4 times using a 100-kDa filter (Microcon YM-100, Millipore) to remove excess dye, and incubated with N2a cells cultured in 35 mm glass base dishes (Fig. 6A). Exosome-free PBS(-) that received the same treatment as above was used as a control. The cells were observed at 1, 7, and 24 hr under confocal microscopy.

1. Hardy, J. Amyloid, the presenilins and Alzheimer's disease. *Trends Neurosci.* **20**, 154–159 (1997).
2. Selkoe, D. J. The cell biology of beta-amyloid precursor protein and presenilin in Alzheimer's disease. *Trends Cell Biol.* **8**, 447–453 (1998).
3. Iwata, N., Higuchi, M. & Saido, T. C. Metabolism of amyloid-beta peptide and Alzheimer's disease. *Pharmacol. Ther.* **108**, 129–148 (2005).
4. Iwata, N. *et al.* Metabolic regulation of brain Abeta by neprilysin. *Science* **292**, 1550–1552 (2001).
5. Iwata, N. *et al.* Identification of the major Abeta1-42-degrading catabolic pathway in brain parenchyma: suppression leads to biochemical and pathological deposition. *Nat. Med.* **6**, 143–150 (2000).
6. Yasojima, K., Akiyama, H., McGeer, E. G. & McGeer, P. L. Reduced neprilysin in high plaque areas of Alzheimer brain: a possible relationship to deficient degradation of beta-amyloid peptide. *Neurosci. Lett.* **297**, 97–100 (2001).
7. Miners, J. S., Barua, N., Kehoe, P. G., Gill, S. & Love, S. Aβ-degrading enzymes: potential for treatment of Alzheimer disease. *J. Neuropathol. Exp. Neurol.* **70**, 944–959 (2011).
8. Sakaguchi, Y., Sekiya, I., Yagishita, K. & Muneta, T. Comparison of human stem cells derived from various mesenchymal tissues: superiority of synovium as a cell source. *Arthritis Rheum.* **52**, 2521–2529 (2005).
9. Banas, A. *et al.* Adipose tissue-derived mesenchymal stem cells as a source of human hepatocytes. *Hepatology* **46**, 219–228 (2007).
10. Chamberlain, G., Fox, J., Ashton, B. & Middleton, J. Concise review: mesenchymal stem cells: their phenotype, differentiation capacity, immunological features, and potential for homing. *Stem Cells* **25**, 2739–2749 (2007).
11. Banas, A., Yamamoto, Y., Teratani, T. & Ochiya, T. Stem cell plasticity: learning from hepatogenic differentiation strategies. *Dev. Dyn.* **236**, 3228–3241 (2007).
12. Sadan, O., Melamed, E. & Offen, D. Bone-marrow-derived mesenchymal stem cell therapy for neurodegenerative diseases. *Expert. Opin. Biol. Ther.* **9**, 1487–1497 (2009).
13. Jin, H. K., Bae, J. S., Furuya, S. & Carter, J. E. Amyloid beta-derived neuroplasticity in bone marrow-derived mesenchymal stem cells is mediated by NPY and 5-HT2B receptors via ERK1/2 signalling pathways. *Cell Prolif.* **42**, 571–586 (2009).
14. Habisch, H. J. *et al.* Efficient processing of Alzheimer's disease amyloid-Beta peptides by neuroectodermally converted mesenchymal stem cells. *Stem Cells Dev.* **19**, 629–633 (2010).
15. Lee, J. K. *et al.* Intracerebral transplantation of bone marrow-derived mesenchymal stem cells reduces amyloid-beta deposition and rescues memory deficits in Alzheimer's disease mice by modulation of immune responses. *Stem Cells.* **28**, 329–43 (2010).
16. Kil, J., Jin, H. K. & Bae, J. S. Bone marrow-derived mesenchymal stem cells reduce brain amyloid-beta deposition and accelerate the activation of microglia in an acutely induced Alzheimer's disease mouse model. *Neurosci. Lett.* **450**, 136–141 (2009).
17. Lee, H. J. *et al.* The therapeutic potential of human umbilical cord blood-derived mesenchymal stem cells in Alzheimer's disease. *Neurosci. Lett.* **481**, 30–35 (2010).
18. Zilka, N. *et al.* Mesenchymal stem cells rescue the Alzheimer's disease cell model from cell death induced by misfolded truncated tau. *Neuroscience* **193**, 330–337 (2011).
19. Katsuda, T., Kosaka, N., Takeshita, F. & Ochiya T. The therapeutic potential of mesenchymal stem cell-derived extracellular vesicles. *Proteomics* (in press).
20. Théry, C., Ostrowski, M. & Segura, E. Membrane vesicles as conveyors of immune responses. *Nat. Rev. Immunol.* **9**, 581–593 (2009).
21. Valadi, H. *et al.* Exosome-mediated transfer of mRNAs and microRNAs is a novel mechanism of genetic exchange between cells. *Nat. Cell Biol.* **9**, 654–659 (2007).
22. Taylor, D. D. & Gercel-Taylor, C. Exosomes/microvesicles: mediators of cancer-associated immunosuppressive microenvironments. *Semin. Immunopathol.* **33**, 441–454 (2011).
23. Kosaka, N. *et al.* Secretory mechanisms and intercellular transfer of microRNAs in living cells. *J. Biol. Chem.* **285**, 17442–17452 (2010).
24. Bruno, S. *et al.* Mesenchymal stem cell-derived microvesicles protect against acute tubular injury. *J. Am. Soc. Nephrol.* **20**, 1053–1067 (2009).
25. Lai, R. C. *et al.* Exosome secreted by MSC reduces myocardial ischemia/reperfusion injury. *Stem Cell Res.* **4**, 214–222 (2010).

26. Miners, J. S., Verbeek, M. M., Rikkert, M. O., Kehoe, P. G. & Love, S. Immunocapture-based fluorometric assay for the measurement of neprilysin-specific enzyme activity in brain tissue homogenates and cerebrospinal fluid. *J. Neurosci. Methods* **167**, 229–236 (2008).
27. Théry, C., Amigorena, S., Raposo, G. & Clayton, A. Isolation and characterization of exosomes from cell culture supernatants and biological fluids. *Curr. Protoc. Cell Biol.* Chapter 3:Unit 3.22 (2006).
28. Taylor, D. D., Zacharias, W. & Gercel-Taylor, C. Exosome isolation for proteomic analyses and RNA profiling. *Methods Mol. Biol.* **728**, 235–246 (2011).
29. Denzer, K., Kleijmeer, M. J., Heijnen, H. F., Stoorvogel, W. & Geuze, H. J. Exosome: from internal vesicle of the multivesicular body to intercellular signaling device. *J. Cell Sci.* **113**, 3365–3374 (2000).
30. Stewart, K. *et al.* STRO-1, HOP-26 (CD63), CD49a and SB-10 (CD166) as markers of primitive human marrow stromal cells and their more differentiated progeny: a comparative investigation in vitro. *Cell Tissue. Res.* **313**, 281–290 (2005).
31. van Niel, G., Porto-Carreiro, I., Simoes, S. & Raposo, G. Exosomes: a common pathway for a specialized function. *J. Biochem.* **140**, 13–21 (2006).
32. Shirotani, K. *et al.* Neprilysin degrades both amyloid beta peptides 1–40 and 1–42 most rapidly and efficiently among thiorphan- and phosphoramidon-sensitive endopeptidases. *J. Biol. Chem.* **276**, 21895–21901 (2001).
33. Trajkovic, K. *et al.* Ceramide triggers budding of exosome vesicles into multivesicular endosomes. *Science* **319**, 1244–1247 (2008).
34. Carlsson, L. *et al.* Characteristics of human prostasomes isolated from three different sources. *Prostate* **54**, 322–330 (2003).
35. Gatti, J. L., Métayer, S., Belghazi, M., Dacheux, F. & Dacheux, J. L. Identification, proteomic profiling, and origin of ram epididymal fluid exosome-like vesicles. *Biol. Reprod.* **72**, 1452–1465 (2005).
36. Conde-Vancells, J. *et al.* Candidate biomarkers in exosome-like vesicles purified from rat and mouse urine samples. *Proteomics* **4**, 416–425 (2010).
37. LaFerla, F. M., Green, K. N. & Oddo, S. Intracellular amyloid-beta in Alzheimer's disease. *Nat. Rev. Neurosci.* **8**, 499–509 (2007).
38. Keyser, K. A., Beagles, K. E. & Kiem, H. P. Comparison of mesenchymal stem cells from different tissues to suppress T-cell activation. *Cell Transplant* **16**, 555–562 (2007).
39. Banas, A. *et al.* IFATS collection: in vivo therapeutic potential of human adipose tissue mesenchymal stem cells after transplantation into mice with liver injury. *Stem Cells* **26**, 2705–2712 (2008).
40. Ahmadian, Kia N. *et al.* Comparative analysis of chemokine receptor's expression in mesenchymal stem cells derived from human bone marrow and adipose tissue. *J. Mol. Neurosci.* **44**, 178–185 (2011).
41. Ikegame, Y. *et al.* Comparison of mesenchymal stem cells from adipose tissue and bone marrow for ischemic stroke therapy. *Cytotherapy* **13**, 675–685 (2011).
42. Cocucci, E., Racchetti, G. & Meldolesi, J. Shedding microvesicles: artefacts no more. *Trends Cell Biol.* **19**, 43–51 (2009).
43. Alvarez-Erviti, L. *et al.* Delivery of siRNA to the mouse brain by systemic injection of targeted exosomes. *Nat. Biotechnol.* **29**, 341–345 (2011).
44. Zhuang, X. *et al.* Zhang HG.Treatment of brain inflammatory diseases by delivering exosome encapsulated anti-inflammatory drugs from the nasal region to the brain. *Mol. Ther.* **19**, 1769–1779 (2011).
45. Hemming, M. L. *et al.* Reducing amyloid plaque burden via ex vivo gene delivery of an Abeta-degrading protease: a novel therapeutic approach to Alzheimer disease. *PLoS Med.* **4**, e262 (2007).
46. Liu, Y. *et al.* Expression of neprilysin in skeletal muscle reduces amyloid burden in a transgenic mouse model of Alzheimer disease. *Mol. Ther.* **17**, 1381–1386 (2009).

Acknowledgements

We thank Drs. Takaomi Saido and Takashi Saito (RIKEN) for providing the N2a cells, Dr. Yukio Kato (Hiroshima University) for providing the human BM-MSCs #1 - #3, Dr. Yoko Kayama and Ms. Noriko Kai (Terabase Inc.) for providing electron microscopy images, Ms. Ayako Irie (Quantum Design Japan, Inc.) for assisting with NTA using the Nanosight system Mr. Ryushi Fukuda (Meiwafosis Co. Ltd) for assisting with the SIOS analysis using the q Nano system, and Ms. Ayako Inoue (National Cancer Center) for her excellent technical assistance. This study was supported in part by a Grant-in-Aid for the Third-Term Comprehensive 10-Year Strategy for Cancer Control of Japan, a grant-in-aid for Scientific Research on Priority Areas Cancer from the Japanese Ministry of Education, Culture, Sports, Science and Technology, a Grant-in-Aid for cancer research promotion from National Cancer Center of Japan, the Program for Promotion of Fundamental Studies in Health Sciences of the National Institute of Biomedical Innovation (NiBio) of Japan, and Grant-in-Aid for Scientific Research on Innovative Areas ("functional machinery for non-coding RNAs") from the Japanese Ministry of Education, Culture, Sports, Science, and Technology.

Author contributions

T.O. supervised the project; T.K., R.T., K.O., F.T., Y.S., M.K. and T.O. designed research; T.K., R.T., Y.Y. and K.T. performed experiments; T.K. and R.T. analyzed data; and T.K., N.K. and T.O. wrote the paper.

Additional information

Supplementary information accompanies this paper at http://www.nature.com/scientificreports

Competing financial interests: The authors declare no competing financial interests.

How to cite this article: Katsuda, T. *et al.* Human adipose tissue-derived mesenchymal stem cells secrete functional neprilysin-bound exosomes. *Sci. Rep.* **3**, 1197; DOI:10.1038/srep01197 (2013).

HEPATOLOGY
Official Journal of the American Association for the Study of Liver Diseases

LIVER INJURY/REGENERATION

Adipose Tissue-Derived Stem Cells as a Regenerative Therapy for a Mouse Steatohepatitis-Induced Cirrhosis Model

Akihiro Seki,[1,2*] Yoshio Sakai,[1,3*] Takuya Komura,[2] Alessandro Nasti,[2] Keiko Yoshida,[2] Mami Higashimoto,[2] Masao Honda,[1] Soichiro Usui,[2] Masayuki Takamura,[2] Toshinari Takamura,[2] Takahiro Ochiya,[4] Kengo Furuichi,[5] Takashi Wada,[3] and Shuichi Kaneko[1,2]

Cirrhosis is a chronic liver disease that impairs hepatic function and causes advanced fibrosis. Mesenchymal stem cells have gained recent popularity as a regenerative therapy since they possess immunomodulatory functions. We found that injected adipose tissue-derived stem cells (ADSCs) reside in the liver. Injection of ADSCs also restores albumin expression in hepatic parenchymal cells and ameliorates fibrosis in a nonalcoholic steatohepatitis model of cirrhosis in mice. Gene expression analysis of the liver identifies up- and down-regulation of genes, indicating regeneration/repair and anti-inflammatory processes following ADSC injection. ADSC treatment also decreases the number of intrahepatic infiltrating $CD11b^+$ and $Gr\text{-}1^+$ cells and reduces the ratio of $CD8^+/CD4^+$ cells in hepatic inflammatory cells. This is consistent with down-regulation of genes in hepatic inflammatory cells related to antigen presentation and helper T-cell activation. *Conclusion*: These results suggest that ADSC therapy is beneficial in cirrhosis, as it can repair and restore the function of the impaired liver. (HEPATOLOGY 2013;58:1133-1142)

Cirrhosis is a serious, life-threatening advanced stage of chronic liver disease that leads to hepatic dysfunction.[1] Cirrhosis frequently develops into hepatocellular carcinoma,[2,3] which exacerbates the prognosis of patients with cirrhosis. The ultimate treatment for cirrhosis is a liver transplant,[4] which can be lethal.[5] The number of donor livers, however, is not sufficient to meet the needs of all transplant patients. Thus, a novel therapy for cirrhosis needs to be developed to improve cirrhotic liver prognosis.

The underlying pathogenesis of chronic liver disease is persistent inflammation. Advanced disease is marked by advanced fibrosis concomitant with distorted liver architecture characterized by regenerative nodules and impaired hepatic function. Advanced fibrosis in the cirrhotic liver is also a risk factor for the development of hepatocellular carcinoma.[6] Treatment of cirrhosis suppresses inflammation by eradicating hepatitis virus infection or reducing liver steatosis in nonalcoholic steatohepatitis (NASH). Decreasing liver inflammation and restoring hepatocyte function improves the prognosis.

Pluripotent mesenchymal stem cells (MSCs) differentiate into adipocyte, chondrocyte, and osteocyte lineages.[7] These cells can also differentiate into other lineages, including neurons[8] and hepatocytes.[9,10] MSCs can also regulate the immune response.[11] Thus, MSCs attract attention as a therapeutic target in the

Abbreviations: ADSCs, adipose-tissue-derived stem cells; AFP, alpha-fetoprotein; Ath+HF, atherogenic high-fat; IL, interleukin; MMP, matrix metalloproteinase; MSC, mesenchymal stem cells; NASH, nonalcoholic steatohepatitis; PBS, phosphate-buffered saline; 18S rRNA, 18S ribosomal RNA; α-SMA, alpha-smooth muscle actin.

From the [1]Department of Gastroenterology, Kanazawa University Hospital, Ishikawa, Japan; [2]Disease Control and Homeostasis, Kanazawa University, Ishikawa, Japan; [3]Department of Laboratory Medicine, Kanazawa University Hospital, Ishikawa, Japan; [4]National Cancer Research Institute, Tokyo, Japan; [5]Division of Blood Purification, Kanazawa University Hospital, Ishikawa, Japan.

Received September 27, 2012; accepted April 15, 2013.

Supported in part by subsidies from the Japanese Ministry of Education, Culture, Sports, Science and Technology and the Japanese Ministry of Health, Labor and Welfare.

*These authors contributed equally to this work.

regeneration or repair of various impaired organs. Mesenchymal tissue from bone marrow, umbilical cord, and adipose tissue are relatively enriched with pluripotent stem cells.[12] Since the pathophysiological features of liver cirrhosis are a consequence of chronic hepatic inflammation, MSCs are especially suited to enhance regeneration and/or repair of damaged cirrhotic liver.

We have established a clinically relevant NASH cirrhotic murine model by feeding animals an atherogenic high-fat (Ath+HF) diet.[13] In this study we examined whether adipose-tissue-derived stem cells (ADSCs) can regenerate and/or repair the cirrhotic liver. We observed that injected ADSCs resided in the liver and expressed albumin, leading to restored albumin expression in hepatic parenchymal cells. ADSCs also ameliorated advanced fibrosis. Moreover, ADSCs suppressed the underlying persistent inflammation contributed by granulocytes, phagocytic cells, and T cells. These results suggest that treatment of patients with cirrhosis with ADSCs is a potentially novel approach for regenerating and/or repairing damaged cirrhotic liver tissue to restore hepatic function.

Materials and Methods

Culture of ADSCs. ADSCs were prepared as described.[14] Briefly, adipose tissue was obtained from the inguinal subcutaneous region of 10-week-old GFP-Tg male mice (a gift from Professor Okabe, Osaka University, Japan). The stem cell fraction was isolated from adipose tissue using type-I collagenase (Wako Pure Chemical Industries, Osaka, Japan) and cultured in Dulbecco's modified Eagle's medium: nutrient mixture F-12 supplemented with 10% heat-inactivated bovine serum albumin and 1% antibiotic-antimycotic solution. Cell culture reagents were purchased from Life Technologies (Carlsbad, CA).

NASH Murine Model. Female 8-week-old C57Bl/6J mice were purchased from Charles River Laboratories Japan (Yokohama, Japan). Mice were fed an Ath+HF diet composed of cocoa butter, cholesterol, cholate, and corticotropin-releasing factor-1 (Oriental Yeast Co., Tokyo, Japan) to induce steatohepatitis as reported previously.[13] Our Institutional Review Board approved the care and use of laboratory animals in all experiments.

ADSC Treatment of NASH Mice. ADSCs were harvested after six to eight passages in culture by treatment with trypsin/EDTA (Life Technologies) and passed through a 100-μm Cell Strainer mesh (BD Biosciences, San Jose, CA). Laparotomy was performed to inject 1×10^5 ADSCs or phosphate-buffered saline (PBS) into the splenic subcapsule. After ADSC treatment, the mice were anesthetized with pentobarbital (40 mg/kg; Kyoritsu Seiyaku, Tokyo, Japan), after which the liver was perfused with PBS and dissected. A portion of liver tissue was homogenized and incubated with type I collagenase (Wako Pure Chemical Industries), and hepatic parenchymal cells and inflammatory cells were separated with Percoll (GE Healthcare UK, Buckinghamshire, UK). $CD4^+$ T cells were isolated from hepatic inflammatory cells using a magnetic sorting system, the $CD4^+$ T cell Isolation Kit II (Miltenyi Biotec, Gladbach, Germany).

Histology and Immunohistochemical Staining. Liver tissue was preserved with formalin for paraffin embedding or embedded in OCT compound and frozen for sectioning (Sakura Finetek Japan, Tokyo, Japan). The frozen liver sections were fixed in acetone and endogenous peroxidase activity blocked with 3% hydrogen peroxide solution. After washing in PBS, the sections were incubated with a rabbit anti-CD11b antibody (BD Pharmingen, San Diego, CA) and a rabbit anti-Gr-1 antibody (eBioscience, San Diego, CA) overnight at 4°C. The slides were then washed and incubated with Histofine mouse MAXPO (Nichirei Bioscience, Tokyo, Japan) for 1 hour at room temperature. The immune complex was visualized by incubating with diaminobenzidine for 5 minutes. The paraffin-embedded sections were stained with a rabbit-anti-GFP antibody (Millipore, Billerica, MA), a rabbit anti-α-smooth muscle actin (α-SMA) antibody (Abcam, Cambridge, UK), and a rabbit anticollagen IV antibody (Abcam). Secondary antibody development was performed with diaminobenzidine as described above. In some experiments, the sliced

Address reprint requests to: Shuichi Kaneko, 13-1 Takara-machi, Kanazawa, Ishikawa 920-8641, Japan. E-mail: skaneko@m-kanazawa.jp; fax: +81-76-234-4250.

View this article online at wileyonlinelibrary.com.
DOI 10.1002/hep.26470
Potential conflict of interest: Nothing to report.
Additional Supporting Information may be found in the online version of this article.

sections were double-stained with a combination of a goat antimouse serum albumin antibody (Abcam) and a rabbit anti-GFP antibody followed by the secondary antibody and development as described above. To quantify fibrosis, paraffin-embedded sections were stained with Azan and viewed microscopically, after which the stained area was calculated using an image-analysis system (BIOREVO BZ-9000 and BZ-H1C, Keyence Japan, Osaka, Japan).

Flow Cytometry. Isolated hepatic inflammatory cells were incubated in PBS supplemented with 2% bovine serum albumin (Sigma-Aldrich, St. Louis, MO) for 10 minutes at 4°C. The cells were incubated with fluorescein isothiocyanate (FITC)-conjugated anti-CD4 (eBioscience) and phycoerythrin (PE)-conjugated anti-CD8 antibodies (eBioscience) for 30 minutes at 4°C before examination using a FACSCalibur cytometer (BD Biosciences). Similarly, ADSCs were incubated with PE-conjugated CD90 (Beckman Coulter, Fullerton, CA), or PE-conjugated CD105 (Miltenyi Biotec). The data were analyzed using the FlowJo software (Tree Star, Ashland, OR).

DNA Microarray Analysis. Isolated RNAs were amplified and labeled with Cy3 using a QuickAmp Labeling Kit (Agilent Technologies, Santa Clara, CA) in accordance with the manufacturer's protocol. cRNA (825 ng) was hybridized onto a Whole Mouse Genome 4 × 44K Array (Agilent Technologies). The hybridized microarray slide was scanned using a DNA microarray scanner (model G2505B; Agilent Technologies).

Gene expression analysis was carried out using GeneSpring analysis software (Agilent Technologies). Each measurement was divided by the 75th percentile of all measurements in that sample to normalize per chip. Hierarchical clustering and principal component analysis of gene expression was performed. Welch's t test with Benjamini and Hochberg's false-discovery rate were used to identify differentially expressed genes in the groups of interest. Analysis of biological processes was performed using the MetaCore software suite (GeneGo, San Diego, CA). BRB array tools (http://linus.nci.nih.gov/BRB-ArrayTools.html) were also used for unsupervised clustering or one-way clustering analysis. Microarray data were deposited in the NBCI Gene Expression Omnibus (GSE ID: GSE40395).

Statistical Analysis. GraphPad Prism (v. 5.0; GraphPad Software, La Jolla, CA) was used to perform a Mann-Whitney U test to compare data between two groups, and differences were considered statistically significant at $P < 0.05$.

All other materials and methods are described in the Supporting Information.

Results

Characteristics of the NASH Mouse Model. The pathological and clinical features of cirrhosis in patients are not well replicated by the majority of chemically induced murine cirrhotic liver models. We have established steatohepatitis as a cirrhotic liver mouse model by feeding mice an Ath+HF diet.[13] When mice were fed this diet for 34 weeks, hepatocytes developed steatosis, Mallory-Denk bodies, and ballooning (Fig. 1A,B), which are identical to typical pathological features of clinical NASH.[15] Albumin expression in parenchymal cells of the cirrhotic liver significantly decreased in mice fed the Ath+HF diet for 24 weeks (Fig. 1C), while alpha-fetoprotein (AFP) expression was not affected (Fig. 1D). Fibrosis developed and reached maximal levels after 34 weeks of feeding the Ath+HF diet (Fig. 1E,F). Immunohistochemical staining for immunomodulatory cells showed an increased number of Gr-1$^+$ cells in the liver of the steatohepatitis mice fed the Ath+HF diet for 12, 34, and 70 weeks (Fig. 2A,B). The number of CD11b$^+$ cells in the liver also increased and reached maximal levels after 34 weeks of feeding the Ath+HF diet (Fig. 2C,D). Thus, the murine cirrhosis model established by an Ath+HF diet mimics the features of clinical NASH.

Effect of ADSCs Treatment on Liver Albumin Expression and Fibrosis. Adipose tissue contains MSCs, which have the potential to differentiate into several types of cell lineages[10,14] and to act as immunomodulators.[11] In this study, we isolated stromal cells from inguinal adipose tissue of GFP-expressing transgenic (GFP-Tg) mice as ADSCs and expanded them in culture. The majority of these cells expressed CD90 and CD44, known surface markers of mesenchymal cells (Supporting Fig. 1A). A proportion of the expanded ADSCs also expressed CD105 (Supporting Fig. 1B), which has been recognized as a representative surface marker of MSCs.[11]

We evaluated whether ADSCs could provide a therapeutically beneficial treatment for liver cirrhosis in steatohepatitis mice. We injected 1×10^5 GFP-ADSCs by way of the spleen/portal vein in mice fed the Ath+HF diet for 32 weeks. We observed that the GFP-ADSCs resided in all lobes of the liver at 3, 7, and 14 days after injection (Fig. 3A,B). Importantly, immunohistochemical staining showed that GFP$^+$ cells in the cirrhotic liver expressed higher levels of albumin than did the surrounding parenchymal cells (Fig. 3C).

We also injected 1×10^5 or 2×10^4 GFP-ADSCs twice every 2 weeks by way of the splenic/portal vein

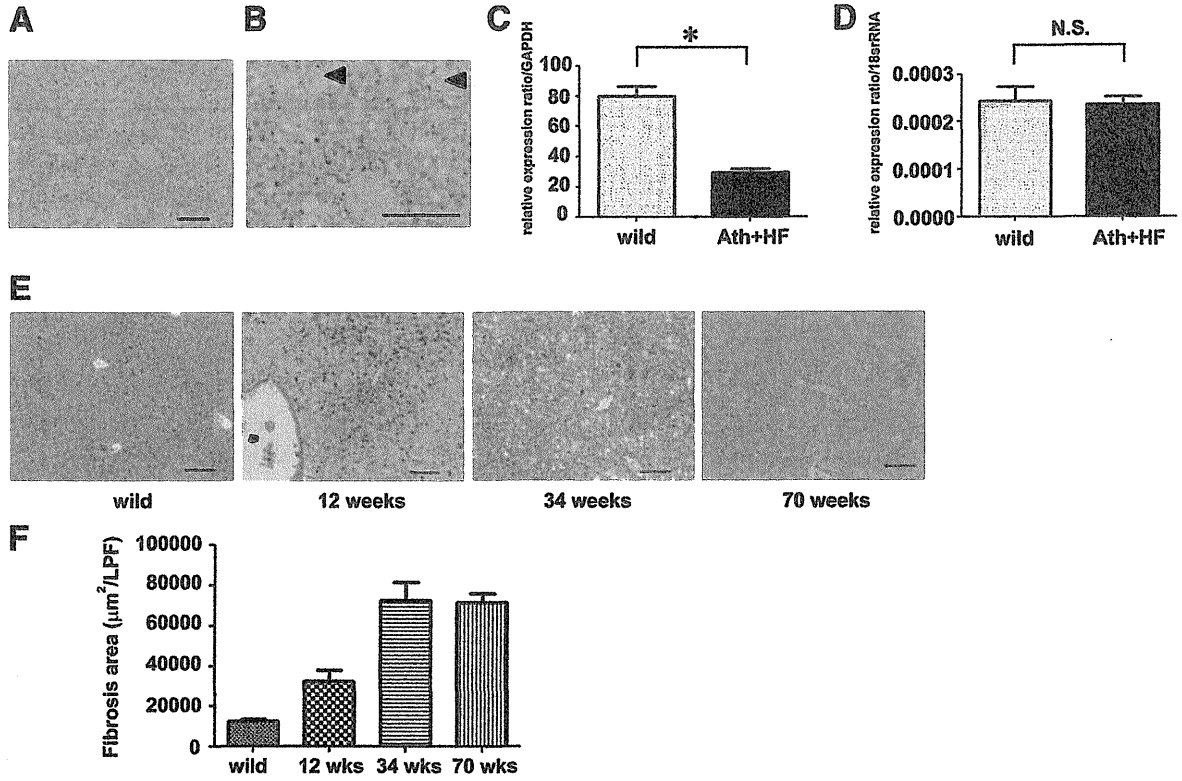

Fig. 1. Characteristics of the steatohepatitis murine model. Eight-week-old C57Bl/6 female mice were fed an Ath+HF diet. Liver tissue was obtained after 34 weeks, sectioned, and histologically examined with hematoxylin and eosin staining in (A,B) mice fed an Ath+HF diet for 34 weeks. Arrowheads indicate a Mallory-Denk body in a hepatocyte with ballooning. Parenchymal cells were isolated from 32-week-old C57Bl/6 wild-type female mice or Ath+HF mice that started the diet at 8 weeks old and continued for 24 weeks. Expression of (C) albumin and (D) AFP was assessed by reverse-transcription polymerase chain reaction (RT-PCR), n = 4, $*P < 0.05$. (E) Fibrosis was histologically examined with Azan staining in liver tissue of mice fed the Ath+HF diet for 12, 34, and 70 weeks. (F) Fibrosis areas of mice at 12, 34, and 70 weeks per ×100 low-power field were calculated for five visual fields. Bars: standard error. Scale bars = 100 μm.

in mice fed an Ath+HF diet for 32 or 36 weeks, respectively. Two weeks after the last injection the mice were euthanized and the therapeutic effects were assessed. The expression of albumin (Fig. 4A) was restored in hepatic parenchymal cells of cirrhotic mice at 2 weeks after the last injection, suggesting that ADSC treatment restored parenchymal cell function. The expression of AFP was also increased by ADSC treatment (Fig. 4B), implying enhanced regeneration of hepatic parenchymal cells. Similar effects were observed with a reduced number of (2×10^4) GFP-ADSCs (Supporting Fig. 2A,B).

We also assessed the effect of ADSC injection on fibrosis in cirrhotic mice. Liver tissue stained with Azan and anticollagen type IV antibody showed that ADSC administration reduced fibrosis compared to control animals (Fig. 5A,B; Supporting Fig. S3A,B). We also evaluated immunohistochemical staining of α-SMA, a marker of stellate cells, which are largely responsible for developing fibrosis. These results demonstrated that the number of α-SMA$^+$ cells was reduced by ADSC treatment (Fig. 5C-E), suggesting that ADSCs suppress the activity of stellate cells and ameliorate liver fibrosis.

Gene Expression Profiling of Cirrhotic Livers Following ADSC Treatment. We examined the gene expression profile of the livers in the NASH mouse model of cirrhosis by DNA microarray to determine whether administration of ADSCs was therapeutically beneficial. We identified expression of 1,249 gene probes that were significantly affected by ADSC injection. Clustering analysis of gene expression using these gene probes distinguished between ADSCs-treated mice and PBS-treated mice (Fig. 6A). Among 1,249 genes, 797 were up-regulated and 452 were down-regulated by ADSC treatment. Regarding matrix metalloproteinase (MMP), expressions of MMP-8 and MMP-9 were enhanced in the liver of NASH mice treated with PBS compared to the wild type; this enhancement was removed by ADSC treatment

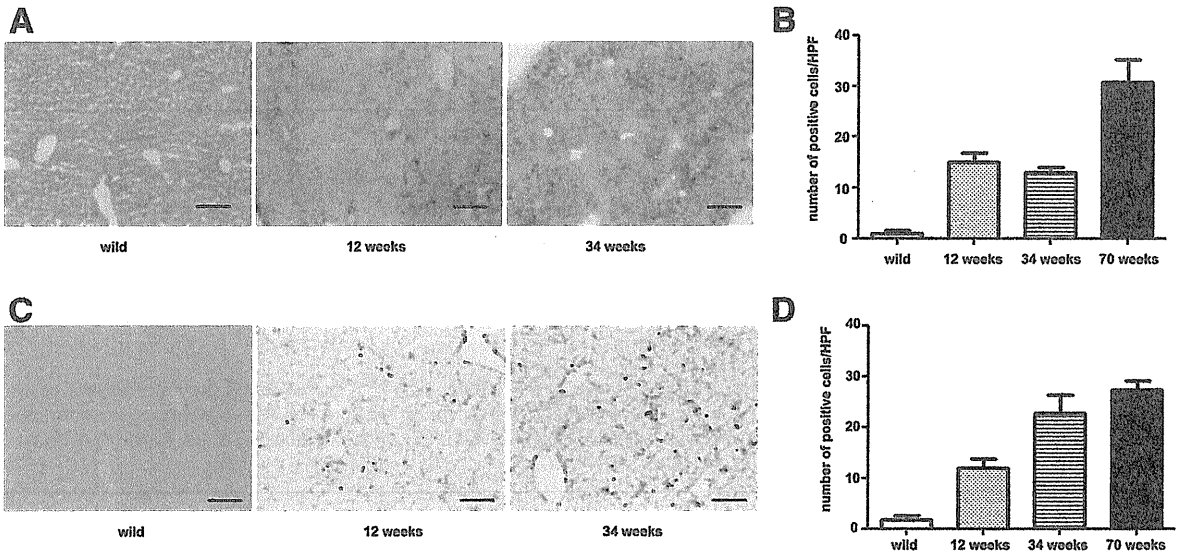

Fig. 2. Immunohistochemical staining of a steatohepatitis liver. Eight-week-old female C57Bl/6 female mice were fed an Ath+HF diet. Liver tissue was obtained from these mice or from wild-type animals after 12, 34, and 70 weeks. Immunohistochemical staining was performed for (A) Gr-1^+ or (C) $CD11b^+$ cells and the number of positive cells in a high-power field was counted for five visual fields for (B) Gr-1 or (D) CD11b at each timepoint.

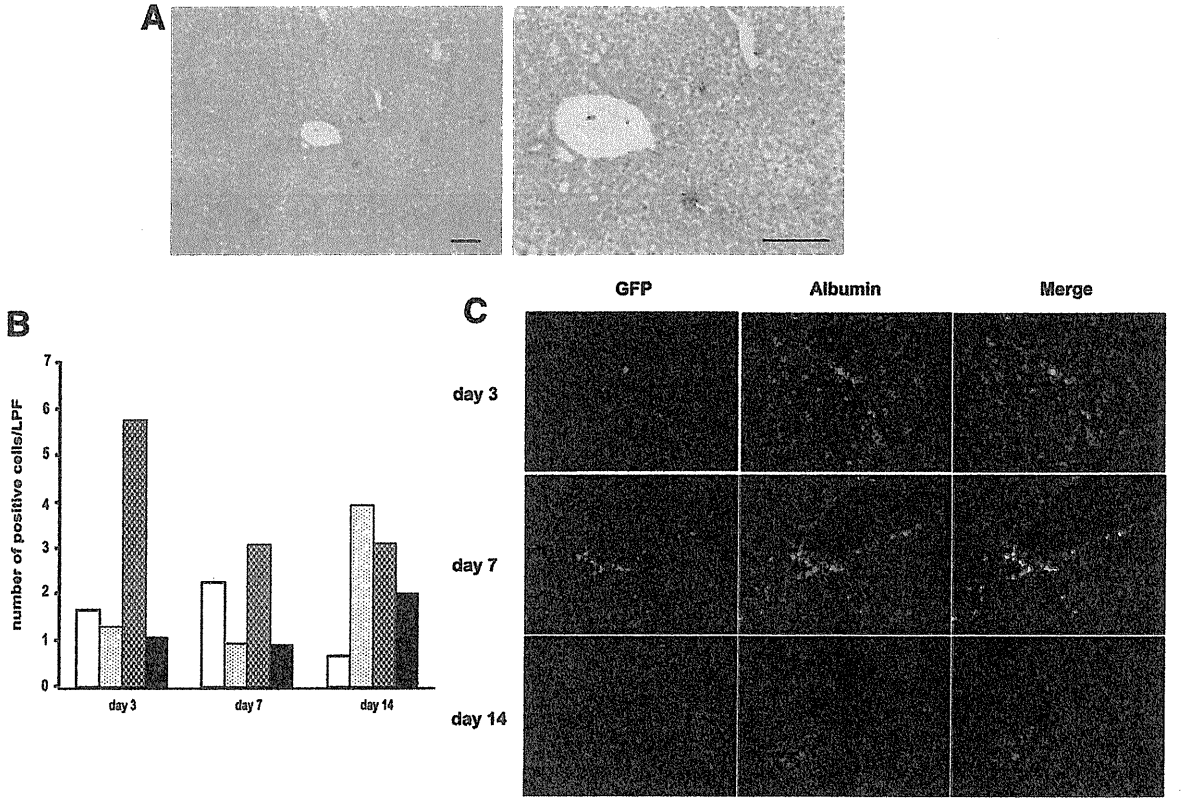

Fig. 3. Distribution of ADSCs and albumin expression in the livers of steatohepatitis mice. ADSCs from GFP-Tg mice (1×10^5) were injected into the splenic subcapsule of cirrhotic C57Bl/6 mice fed the Ath+HF diet for 32 weeks. After 3, 7, and 14 days, liver tissue was obtained and examined by immunohistochemical staining for (A) GFP; Scale bars = 100 μm. (B) GFP^+ cells in the liver were counted per ×100 low-power field and five visual fields were calculated. White bar, caudate lobe; dotted bar, left lobe; hatched bar, middle lobe; black bar, right lobe. (C) Immunohistochemical staining for GFP or albumin antibody. Magnification, ×100.

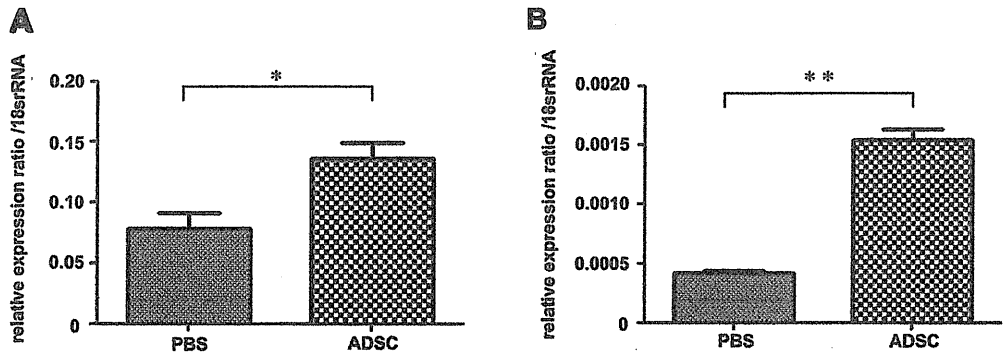

Fig. 4. Albumin and AFP expression in hepatic parenchymal cells. ADSCs from GFP-Tg mice (1×10^5) were injected twice every 2 weeks into the splenic subcapsule of cirrhotic C57Bl/6 mice fed an Ath+HF diet for 32 weeks. Control mice received PBS injections. Two weeks after the last injection, liver tissue was obtained and parenchymal cells were isolated for real-time PCR. Expressions of (A) albumin and (B) AFP were normalized relative to that of 18S ribosomal RNA (rRNA); $^*P < 0.05$, $^{**}P < 0.01$.

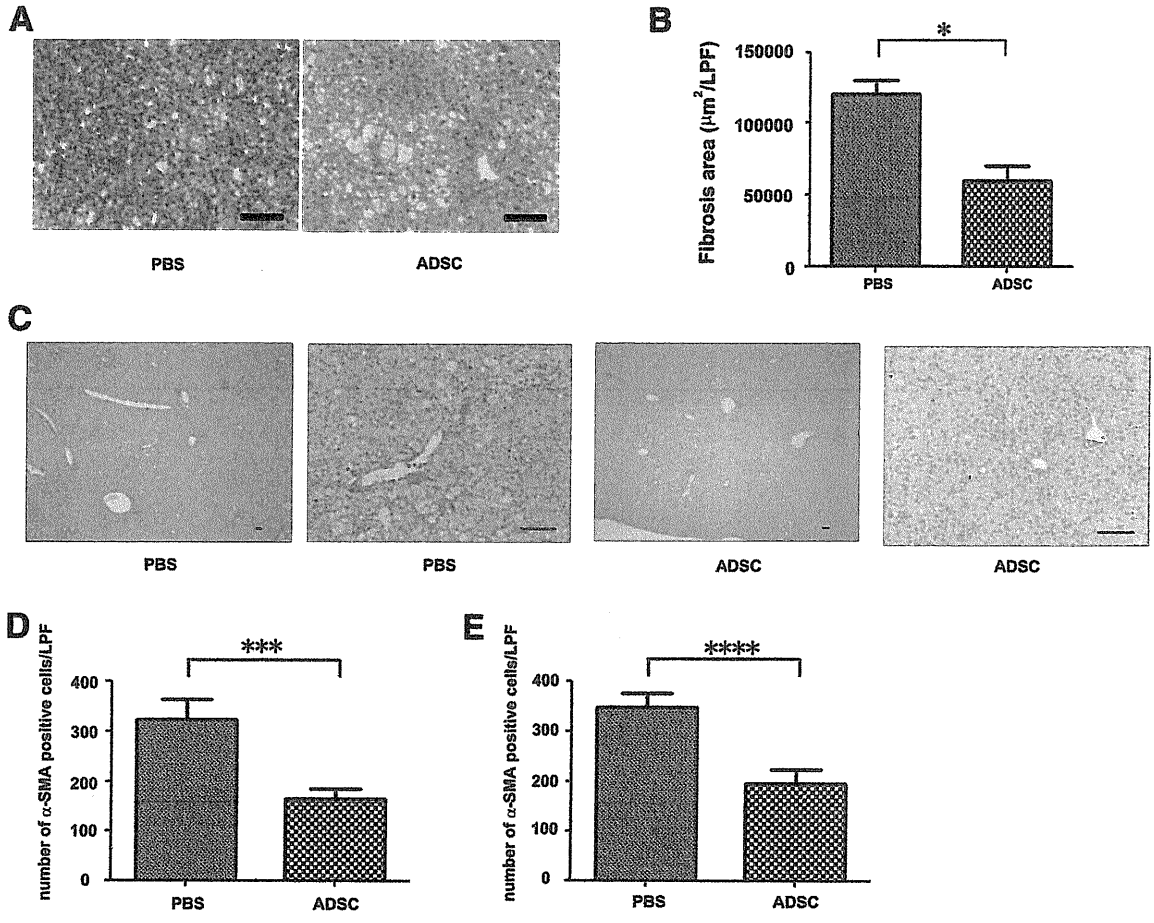

Fig. 5. Effect of ADSCs on liver fibrosis. ADSCs from GFP-Tg mice (1×10^5) were injected twice every 2 weeks into the splenic subcapsule of cirrhotic C57Bl/6 mice fed the Ath+HF diet for 32 weeks. Control mice received PBS injections. (A) Two weeks after the last injection, liver tissue was obtained, sectioned, and histologically examined with hematoxylin and eosin staining. (B) Fibrosis was examined by Azan staining and fibrotic area was quantified by image-analysis. (C) Immunohistochemical staining of liver sections for α-SMA. Scale bars = 100 μm. (D,E) The number of α-SMA+ cells in liver tissues obtained 1 (D) or 2 weeks (E) after the last ADSC injection determined by microscopy of five low-power fields (×100); $^{***}P < 0.005$, $^{****}P = 0.0001$.

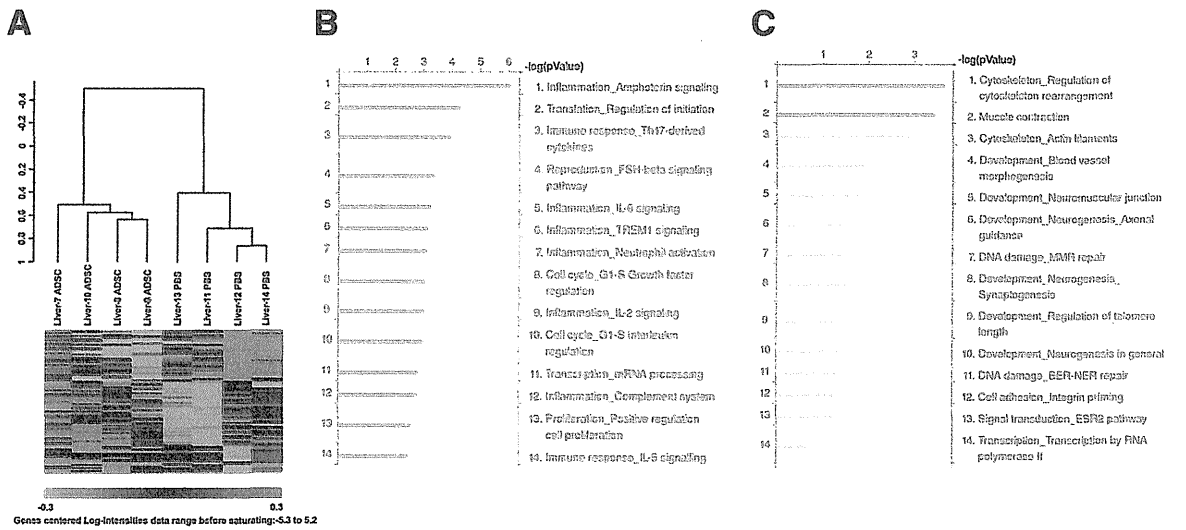

Fig. 6. Hepatic gene expression analysis. ADSCs from GFP-Tg mice (1×10^5) were injected twice every 2 weeks into the splenic subcapsule of cirrhotic C57Bl/6 mice fed an Ath+HF diet for 40 weeks. Control mice received PBS injections. Two weeks later, liver tissue was subjected to RNA isolation and gene expression using DNA microarrays. (A) Unsupervised clustering analysis was performed using probes for 1,249 genes whose expression differed significantly between the PBS and ADSC groups. (B) The biological processes of 452 genes whose expression was down-regulated in the ADSCs group compared to the PBS group were analyzed. (C) The biological processes of 797 genes whose expression was up-regulated in the ADSCs group compared to the PBS group were analyzed.

(Supporting Fig. S4). Biological process analysis indicated that the down-regulated genes were primarily related to inflammation and the immune response (Fig. 6B), and the up-regulated genes were related to tissue construction and development (Fig. 6C). Thus, gene expression analysis of liver tissue demonstrated that ADSCs treatment caused anti-inflammatory effects, as well as regeneration/repair effects, in the livers of a NASH mouse model of cirrhosis.

Anti-inflammatory Effects of ADSC Treatment. The fundamental underlying pathophysiology of steatohepatitis-induced cirrhosis is persistent hepatic inflammation caused by steatosis in hepatocytes.[16] We examined how ADSCs affected persistent inflammation of the liver in NASH mice at 2 weeks after the last injection of ADSCs. Immunohistochemical staining showed that the number of $CD11b^+$ cells accumulating in the livers of cirrhotic mice decreased with ADSC treatment compared to those of PBS-treated mice (Fig. 7A). The number of $Gr\text{-}1^+$ cells in cirrhotic liver also decreased with ADSC treatment (Fig. 7A), suggesting that ADSCs affect granulocytes and antigen-presenting cell lineage.

We further examined whether ADSC treatment affected the lymphocyte lineage of T cells, since they also play an important role in immune regulation of steatohepatitis.[17] We isolated lymphocytes from the livers of mice treated with ADSCs and examined the $CD4^+$ and $CD8^+$ T cells using flow cytometry. $CD8^+$ T cells were found predominantly in cirrhotic mice treated with PBS (Fig. 7B,C). However, when the mice were treated with ADSCs the number of $CD4^+$ T cells increased and was comparable to that of $CD8^+$ T cells, indicating that ADSC treatment affected T-cell subpopulations.

Gene Expression Profiling of Hepatic Inflammatory Cells Following ADSC Treatment. We further examined how injected ADSCs affected hepatic inflammatory cell gene expression by using DNA microarrays. By filtering the results from 5,065 gene probes, completely discernible clusters of gene expression were formed between ADSC- and PBS-treated animals (Fig. 8A). We identified the expression of 873 genes that were significantly up-regulated at least 2-fold with ADSC injection and 658 genes that were down-regulated. Most of the chemokines and cytokines whose expression was significantly affected by ADSCs were down-regulated (Supporting Table S1). Using the publicly available gene expression database for hematopoietic cells (GSE27787) and various types of helper T cells (GSE14308), we examined features of these affected genes in the context of immunomodulatory cells. Among the hematopoietic cells, genes with available symbol annotation were predominately $Gr\text{-}1^+$ and $CD11b^+$ cells from granulocyte and macrophage lineages (Fig. 8B). Among helper T-cell populations,

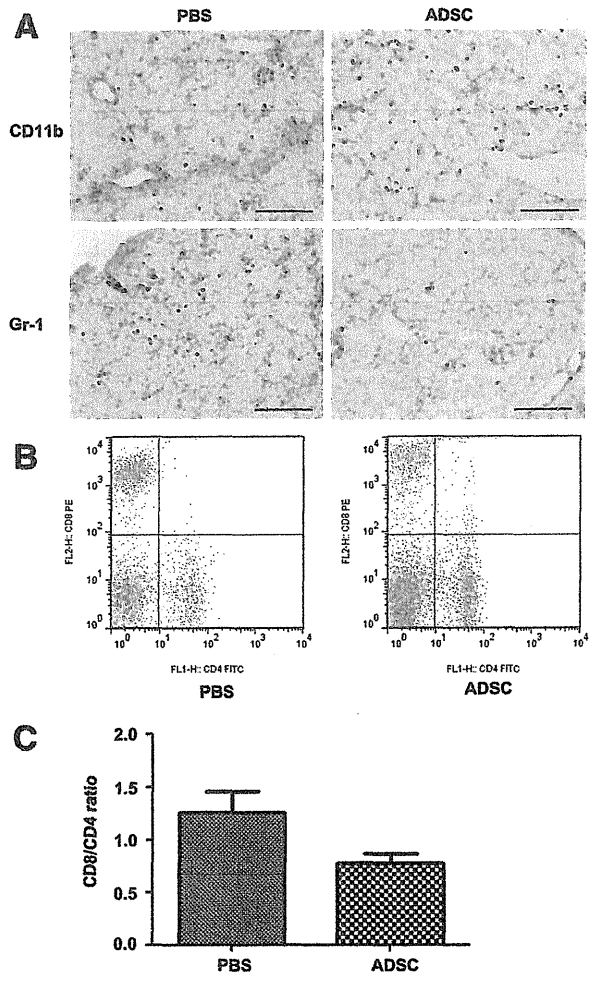

Fig. 7. Effect of ADSCs on inflammatory cells in the cirrhotic liver. ADSCs from GFP-Tg mice (1×10^5) were injected twice every 2 weeks into the splenic subcapsule of cirrhotic C57Bl/6 mice fed the Ath+HF diet for 32 weeks. Control mice received PBS injections. Two weeks later, liver tissue was obtained and immunohistochemical staining of (A) $CD11b^+$ and (B) $Gr\text{-}1^+$ cells was performed. Inflammatory cells in the liver were also isolated and stained with FITC-labeled anti-CD4 and PE-labeled CD8 antibodies. (C) The ratio of $CD8^+$ cells to $CD4^+$ cells was calculated. N = 4 ± standard error.

annotated genes included activated Th1, Th2, and Th17 cell types (Fig. 8C). We also isolated $CD4^+$T cells from hepatic inflammatory cells obtained from NASH mice fed an Ath+HF diet for 12 weeks, then treated with ADSC. Expressions of the Th1, Th2, and Th17 cytokines, interferon-γ, interleukin (IL)−4, IL-10, and IL-17, the Th17-related cytokine transforming growth factor beta (TGF-β), and Foxp3, a representative transcription factor of regulatory T cells, were down-regulated by ADSC treatment (Supporting Fig. S5).

These results suggest that ADSC treatment suppresses inflammation in the NASH mouse model primarily by down-regulating granulocytes, antigen-presenting cells, and activated helper T cells.

Discussion

This study investigated the therapeutic effect of ADSCs in a NASH murine model of cirrhosis. This model is relevant to clinical NASH, with similar pathological features established by an atherogenic high-fat diet, including the appearance of steatosis, ballooning, and Mallory-Denk bodies in hepatocytes, infiltration of inflammatory cells, and pericellular fibrosis. Our results demonstrate that ADSC injection is therapeutically beneficial for cirrhosis in this murine model through restoration of albumin expression in hepatic parenchymal cells, amelioration of fibrosis, and suppression of persistent hepatic inflammation.

Gene expression analysis of the liver in this cirrhotic mouse model revealed that ADSC injection affects biological processes relating to anti-inflammatory and regeneration/repair pathways. The anti-inflammatory effects are mediated by ADSC targeting of $Gr\text{-}1^+$, $CD11b^+$, and helper T-cell lineages. In patients with clinical NASH, the ratio of neutrophils to lymphocytes increases,[18] suggesting that granulocytes are involved in the pathogenesis of NASH. The NASH murine model used in this study produced an increased $CD8^+/CD4^+$ T-cell ratio, which is also comparable to clinical NASH patient pathology.[19] Gene expression analysis of liver tissue and hepatic inflammatory cells from NASH mice showed that Th1-, Th2-, and Th17-related genes were down-regulated by ADSC treatment. Helper T-cell activation skewed to produce Th1 cytokines is pathogenic in steatohepatitis.[20,21] In particular, Th17 is emerging as an important source of IL-17 family cytokines[22] and is involved in the hepatic inflammation in NASH.[23] Helper T cells producing Th2 cytokines such as IL-4, 5, and 13 contribute to fibrosis.[24] We conclude that activated T helper cells are responsible for the pathogenesis of steatohepatitis in the NASH murine model used in this study and that ADSCs suppress pathogenic helper T-cell activation. However, the suppression of miscellaneous effector and regulatory helper T cells by ADSCs should be further evaluated with regard to prevention of hepatocellular carcinoma, a frequent sequela to cirrhosis, since Th1 promotes antitumor immunity and Th2 down-regulates antitumor immunity.

We also observed that ADSC treatment ameliorated fibrosis and decreased the number of α-SMA^+ stellate

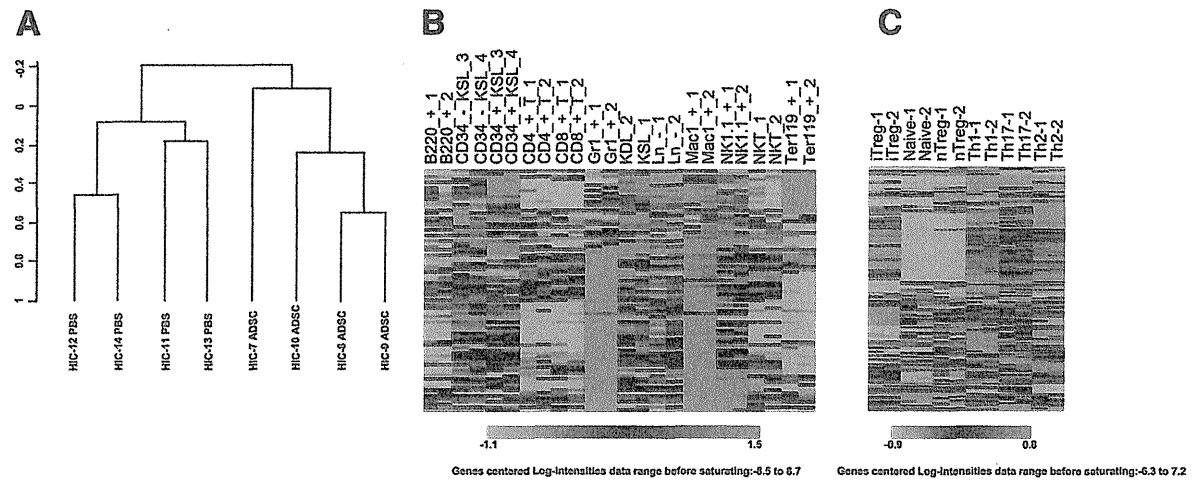

Fig. 8. Gene-expression analysis of intrahepatic inflammatory cells. ADSCs from GFP-Tg mice (1×10^5) were injected twice every 2 weeks into the splenic subcapsule of cirrhotic C57Bl/6 mice fed an Ath+HF diet for 40 weeks. Control mice received PBS injections. Inflammatory cells were isolated from the liver and gene expression examination was performed using DNA microarrays. (A) Unsupervised clustering analysis using the filtered 5,065 gene probes. HIC; hepatic inflammatory cells. (B) One-way clustering analysis using a publicly available database of hematopoietic cells (GSE27787) of 658 genes whose expression was down-regulated by ADSC treatment with available gene symbol annotations. (C) One-way clustering analysis using publicly available database of different helper T subsets (GSE14308) of 658 genes whose expression was down-regulated by ADSCs treatment with available gene symbol annotations.

cells in cirrhotic liver. When inflammation persists in the liver, fibrosis progresses due to these activated stellate cells, which are almost identical to myofibroblasts and produce extracellular matrix. Stellate cells are activated by miscellaneous factors including TGF-β and platelet-derived growth factor,[25] produced mostly from Kupffer cells. Helper T cells expressing Th2 cytokines are also involved in the development of fibrosis. Gene expression analysis of the cirrhotic livers indicated that ADSC treatment suppressed Th2-type helper T cells. Although details of how these molecules mediate fibrosis development have yet to be examined in the current NASH murine model, the antifibrotic effect of ADSCs is achieved in part by suppressing Th2-type helper T cells. We found that MMP-8 and MMP-9 enhancement in the NASH-cirrhotic liver was ameliorated by ADSC treatment. MMP-9 expression is related to the inflammation typical of steatohepatitis[26] and can ameliorate the hepatic fibrosis induced by carbon tetrachloride.[27] Further studies are needed to clarify the role of MMPs in the pathogenesis of cirrhosis as well as to explore novel therapies for this condition.

Pluripotent MSCs differentiate into several cell lineages and are a promising avenue for regenerative therapy of various impaired organs, including the liver. Although ADSCs were observed in cirrhotic livers at up to 2 weeks after injection and expressed albumin, the numbers of resident cells were not sufficient to supplement hepatic function. Therefore, pluripotency, as well as the anti-inflammatory and antifibrotic effects of ADSCs, are important for their regenerative/repair effects in liver cirrhosis. Rather than studying the effects of ADSCs on early-stage steatohepatitis, we treated mice with endstage cirrhosis with ADSCs to observe their therapeutic effects. Our results demonstrated that ADSCs can effectively resolve chronic fibrosis and decrease inflammation, thereby restoring hepatic function in endstage cirrhotic mice, implying the usefulness of this therapy as an alternative to liver transplantation.

In conclusion, ADSCs proved therapeutically beneficial and clinically relevant in regenerative therapy of a murine steatohepatitis-cirrhosis model. Clinical application of ADSCs in the treatment of cirrhosis is expected to provide a novel alternative regenerative/repair therapy for patients with cirrhosis.

References

1. D'Amico G, Garcia-Tsao G, Pagliaro L. Natural history and prognostic indicators of survival in cirrhosis: a systematic review of 118 studies. J Hepatol 2006;44:217-231.
2. Llovet JM, Burroughs A, Bruix J. Hepatocellular carcinoma. Lancet 2003;362:1907-1917.
3. Fattovich G, Stroffolini T, Zagni I, Donato F. Hepatocellular carcinoma in cirrhosis: incidence and risk factors. Gastroenterology 2004;127:S35-50.
4. Kamath PS, Kim WR. The model for end-stage liver disease (MELD). HEPATOLOGY 2007;45:797-805.
5. Stravitz RT, Carl DE, Biskobing DM. Medical management of the liver transplant recipient. Clin Liver Dis 2011;15:821-843.